Engineering Model for Predicting the Intradiffusion Coefficients of Hydrogen and Oxygen in Vapor, Liquid, and Supercritical Water based on Molecular Dynamics Simulations

Tsimpanogiannis, Ioannis N.; Maity, Samadarshi; Celebi, Alper T.; Moultos, Othonas A.

DOI
10.1021/acs.jced.1c00300

Publication date
2021

Document Version
Final published version

Published in
Journal of Chemical and Engineering Data

Citation (APA)
Tsimpanogiannis, I. N., Maity, S., Celebi, A. T., & Moultos, O. A. (2021). Engineering Model for Predicting the Intradiffusion Coefficients of Hydrogen and Oxygen in Vapor, Liquid, and Supercritical Water based on Molecular Dynamics Simulations. *Journal of Chemical and Engineering Data*, *66*(8), 3226-3244. https://doi.org/10.1021/acs.jced.1c00300

Journal of Chemical&Engineering Data

pubs.acs.org/jced Article

Engineering Model for Predicting the Intradiffusion Coefficients of Hydrogen and Oxygen in Vapor, Liquid, and Supercritical Water based on Molecular Dynamics Simulations

Ioannis N. Tsimpanogiannis,* Samadarshi Maity, Alper T. Celebi, and Othonas A. Moultos*

Cite This: *J. Chem. Eng. Data* 2021, 66, 3226−3244 Read Online

ACCESS | Metrics & More | Article Recommendations | Supporting Information

ABSTRACT: Molecular dynamics simulations are carried out to compute the intradiffusion coefficients of H_2 and O_2 in H_2O for temperatures ranging from 275.15 to 975.15 K and pressures ranging from 0.1 to 200 MPa. These conditions span vapor, liquid, and supercritical conditions. For the vast majority of the state points examined, experimental data are not available. The accuracy of six H_2 and six O_2 force fields is tested in reproducing the available experimentally measured densities, self-diffusivities, and shear viscosities of the pure gas and the intradiffusivity of the gas in H_2O. Namely, we screen the H_2 force fields developed by Buch, Vrabec and co-workers, Hirschfelder et al., Cracknell, a modified Silvera−Goldman, and Marx and Nielaba. For O_2, the force fields by Bohn et al., Miyano, Coon et al., Hansen et al., Vrabec et al., and Watanabe are tested. Overall, the force fields by Buch and Bohn for H_2 and O_2, respectively, were found to perform the best, and combined with the TIP4P/2005 H_2O force field are used to compute the intradiffusivities in the entire temperature and pressure range. The new data are used to develop an engineering model that can predict the H_2 and O_2 intradiffusivity in vapor, liquid, and supercritical H_2O. The new model uses 11 parameters and has an accuracy of 4−11%. The model is validated with other available experimental and simulation data for H_2 and O_2 in H_2O and pure H_2O. Aside from the extensive collection of new data for the intradiffusivities of H_2 and O_2 in H_2O, we present new data for the densities, shear viscosities, and self-diffusivities of pure TIP4P/2005 H_2O in the same wide temperature and pressure range. The new data and the engineering model presented here can be used for the design and optimization of chemical processes, for which the knowledge of H_2 and O_2 diffusivities in H_2O is important.

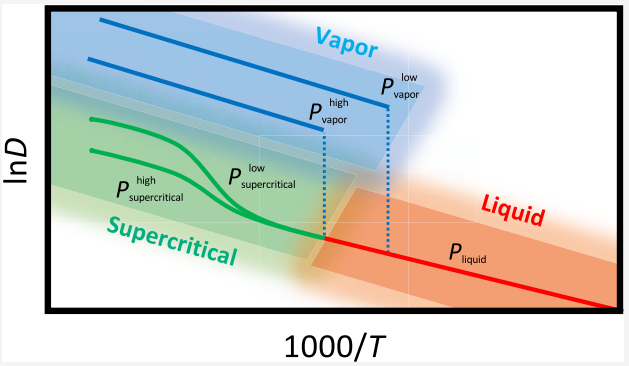

1. INTRODUCTION

The diffusivity of H_2 and O_2 in H_2O is encountered in numerous environmental, geological, industrial, and biological systems. For example, the diffusion process of light, sparingly soluble gas in H_2O is the major controlling parameter during the air−water gas exchange.[1] Typical applications of industrial interest involving H_2 and/or O_2 diffusion in H_2O are the low-to-moderate temperature processes encountered in fuel cells[2] and H_2O electrolysis,[3] the low[4] and moderate/high[5,6] temperature water−gas shift reactions taking place during biomass gasification, and the supercritical H_2O oxidation, which is considered an innovative green technology for the treatment of industrial waste and sludge.[7,8]

The design and optimization of these processes require the knowledge of the intradiffusion coefficients of H_2 and/or O_2 in H_2O in a wide range of conditions, covering the gas, liquid, and supercritical regions. Experimental measurements are often available, albeit only for a limited number of state points, usually at atmospheric pressure.[9] For this reason, semi-empirical correlations have been extensively used for obtaining the diffusivity values at conditions outside the range of experimental measurements.[10−17] For an extensive discussion on the various correlations, the reader is referred elsewhere.[11,15,18] Despite being fast and easy to use, these correlations depend on the quality of the available experimental data, while they provide limited physical insight into the transport mechanisms taking place. To this end, molecular dynamics (MD) simulations are used as a complementary approach for computing diffusivities when experimental data are not available.[19,20] In the past few decades, MD simulations have played a pivotal role in science and engineering since they provide a fundamental understanding of phenomena and processes at the molecular level.[21,22] The advent of faster computers and more efficient algorithms has resulted in the extensive use of MD simulations

Received: April 25, 2021
Accepted: June 14, 2021
Published: July 5, 2021

https://doi.org/10.1021/acs.jced.1c00300
J. Chem. Eng. Data 2021, 66, 3226−3244

for computing the thermodynamic, transport, and structural properties of pure components and mixtures relevant to industrial applications.[23] A number of MD simulation studies of the intradiffusivity of H_2[24−27] and O_2[24,28−33] in H_2O have been reported. However, these studies are mostly limited to supercritical H_2O conditions, with only a few considering lower pressures and temperatures, e.g., the study by Thapa and Adhikari on O_2 diffusivity in H_2O at 0.1 MPa and temperatures up to 306 K.[34]

Thus, a dataset of H_2 and O_2 intradiffusivities in H_2O spanning the liquid, vapor, and supercritical conditions is largely lacking. The main objective of this study is twofold: (a) to provide a reliable set of intradiffusivity data for infinitely diluted H_2 and O_2 in H_2O for temperatures and pressures in the range of 275.15−975.15 K and 0.1−200 MPa, respectively, and (b) to establish an engineering model with few parameters that can be used to accurately predict these diffusivities for any pressure and temperature. To this purpose, a screening of six H_2 and six O_2 force fields is performed. One force field for each gas is selected based on their performance in predicting the available experimentally measured densities, shear viscosities and self-diffusion coefficients of the pure gas, and the intradiffusion coefficients of gas into H_2O. The selected force fields are then combined with the widely used TIP4P/2005 force field[35] to compute the intradiffusion coefficients of H_2 and O_2 in H_2O, at conditions spanning the vapor, liquid, and supercritical regions, for which experimental data are mostly lacking. Due to the extensive number of MD simulations performed in this study, the densities, shear viscosities, and self-diffusivities of the pure TIP4P/2005 H_2O force field are also reported for the whole temperature and pressure range and used to validate the proposed engineering model. The use of the TIP4P/2005 force field to compute the self-diffusion coefficients of pure H_2O has been reviewed in recent studies.[36,37]

The paper is organized as follows. In Section 2, the methods and computational details are described. In Section 3, we discuss the force field validation, the MD results for the diffusivity of H_2 and O_2 in H_2O, and the details of the proposed engineering method. In Section 4, the conclusions are presented.

2. METHODOLOGY

2.1. Force Fields. For modeling H_2, the single-site force fields developed by Buch,[38] Vrabec and co-workers,[39] and Hirschfelder et al.,[40] the two-site force field by Cracknell,[41] and the modified three-site Silvera−Goldman by Alavi et al.,[42] and Marx and Nielaba[43] force fields are tested (for brevity these force fields are referred to as Buch, Vrabec, Hirschfelder, Cracknell, Silvera−Goldman, and Marx hereafter). These H_2 force fields have been recently used in the literature to predict the thermophysical properties of H_2O/H_2 mixtures in a wide range of temperatures and pressures.[39,44,45] Furthermore, the modified Silvera−Goldman force field has been used extensively in MD[42,46] and Monte Carlo[47−49] studies related to H_2 storage in clathrate hydrate structures. For additional information on the performance of the H_2 force fields for various mixtures, conditions, and properties, the reader is referred to the recent studies by Yang et al.[50] and Bartolomeu et al.[51,52] For O_2, the two-site force fields developed by Bohn et al.,[53] Miyano,[54] and Coon et al.,[55] and the three-site models developed by Hansen et al.,[56] Vrabec et al.,[57] and Watanabe[58] are used (for brevity these force fields are referred to as Bohn, Miyano, Coon, Hansen, Vrabec, and Watanabe hereafter). The TIP4P/2005 model[35] is used to model H_2O. Previous studies have shown that the TIP4P/2005 force field can accurately capture the transport properties of pure H_2O and aqueous solutions for a broad range of conditions.[36,59−66] Table 1 lists all of the components simulated in this study and the force fields used for each one component. All force field details are provided in the Supporting Information (Tables S1−S3).

Table 1. Chemical Formulas and Force Fields of the Components Simulated in this Work

component	chemical formula	CAS number	force field
water	H_2O	7732-18-5	TIP4P/2005[35]
hydrogen	H_2	133-74-0	Buch[38]
hydrogen	H_2	133-74-0	Vrabec[39]
hydrogen	H_2	133-74-0	Hirschfelder[40]
hydrogen	H_2	133-74-0	Cracknell[41]
hydrogen	H_2	133-74-0	Silvera−Goldman (modified)[42]
hydrogen	H_2	133-74-0	Marx[43]
oxygen	O_2	7782-44-7	Bohn[53]
oxygen	O_2	7782-44-7	Miyano[54]
oxygen	O_2	7782-44-7	Coon[55]
oxygen	O_2	7782-44-7	Hansen[56]
oxygen	O_2	7782-44-7	Vrabec[57]
oxygen	O_2	7782-44-7	Watanabe[58]

2.2. Molecular Dynamics Simulation Details. The open-source Large-scale Atomic/Molecular Massively Parallel Simulator (LAMMPS)[67] is used for the MD simulations. Periodic boundary conditions are imposed in all directions. The velocity-Verlet algorithm is used to integrate the equations of motion with a time step of 1 fs. For the two-site H_2, two-site O_2, and H_2O force fields, the bond lengths and the angle in H_2O are fixed using the SHAKE algorithm in LAMMPS.[67,68] The three-site H_2 and O_2 force fields are modeled as rigid bodies using the technique developed by Zhang and Glotzer.[69] Thus, in all simulations, the intramolecular interactions are neglected. Only Lennard-Jones (LJ) and Coulombic potentials are used to describe the intermolecular interactions. The cutoff radii for both the LJ and electrostatic energies are set according to the original H_2, O_2, and H_2O force fields. The particle−particle particle−mesh (PPPM)[22,70] method with a relative error of 10^{-5} is used to compute the long-range electrostatic energies. Analytic tail corrections are applied to the energy and pressure. The Lorentz−Berthelot combining rules are used for the interactions between unlike species.[21,22]

The MD simulations are carried out following the procedure described in detail in the Supporting Information of ref 71, i.e., initially, the system is energy minimized, consequently, equilibration runs are performed in the NpT and NVT ensembles for 1−2 ns, and finally the properties are sampled from production runs in the NVE ensemble. The total simulation time of the production runs is in the range of 2−200 ns for obtaining properly converged mean-squared-displacements (MSD) for the computation of the transport coefficients.[71] The temperature and pressure are maintained constant using the Nosé−Hoover thermostat and barostat[21,22] with coupling constants equal to 100 and 1000 fs, respectively. The modifications to the Nosé−Hoover thermostat and the barostat proposed by Kamberaj[72] are used in LAMMPS for the simulations of rigid bodies. All initial configurations are created using PACKMOL software.[73]

https://doi.org/10.1021/acs.jced.1c00300
J. Chem. Eng. Data 2021, 66, 3226−3244

2.3. Computation of Transport Properties. The OCTP (On-the-fly computation of transport properties) plugin[71] in LAMMPS is used to compute the self- and intradiffusivities and shear viscosities from the Einstein relations[20−22,71,74−76] shown in eqs 1 and 2, combined with the order-n algorithm as implemented by Dubbeldam et al.[77]

$$D_i = \lim_{t\to\infty} \frac{1}{6N_i t} \left\langle \sum_{j=1}^{N_i} (\boldsymbol{r}_{j,i}(t) - \boldsymbol{r}_{j,i}(0))^2 \right\rangle \tag{1}$$

where D_i is the self-diffusivity (or intradiffusivity in the case of mixtures) of species i, $\boldsymbol{r}_{j,i}(t)$ is the position of the jth molecule of species i at time t, and N_i is the number of molecules of species i in the system.

$$\eta = \lim_{t\to\infty} \frac{1}{10{\cdot}2t} \frac{V}{k_B T} \left\langle \sum_{\alpha\beta} \left(\int_0^t P_{\alpha\beta}^{os}(t')\mathrm{d}t' \right)^2 \right\rangle \tag{2}$$

where[76,78]

$$P_{\alpha\beta}^{os} = \frac{P_{\alpha\beta} + P_{\beta\alpha}}{2} - \delta_{\alpha\beta}\left(\frac{1}{3}\sum_k P_{kk}\right) \tag{3}$$

where η is the shear viscosity, V is the volume of the system, k_B is the Boltzmann constant, $P_{\alpha\beta}^{os}$ denotes the components of the traceless pressure tensor, $P_{\alpha\beta}$ denotes the off-diagonal components of the pressure tensor, and $\delta_{\alpha\beta}$ is the Kronecker delta. $\langle ... \rangle$ indicates an ensemble average. Although diffusivities and viscosities can also be computed using the Green−Kubo method,[21,22] the use of the Einstein framework has the practical advantage of offering a criterion for specifying the minimum simulation length for obtaining a transport property, i.e., the linear relationship between time and the mean-squared displacement of the dynamical properties of interest is valid at timescales where the slope is 1 in a log−log plot. Such a criterion is not present in the Green−Kubo method, where a time−correlation function slowly converges to zero regardless of the simulation length.[71,79]

In all MD simulations, 1000 H_2O and 5 solute molecules (i.e., H_2 or O_2) are used, corresponding to infinite dilution conditions. As can be seen in Figure S1 in the Supporting Information, the variation in the number of solute molecules (both H_2 and O_2) from 1 to 5 practically yields the same diffusivity values, while the error is reduced by a factor of ca. 2. As shown by Janzen et al.[80] and Guevarra-Carrion et al.,[81] intradiffusion coefficients of mixtures at the infinite dilution limit can also be computed by performing MD simulations at several compositions near the infinite dilution, e.g., x_i = 0.5, 1, 3, and 5 mol %, and extrapolating to $x_i \to 0$. Such an approach may yield relatively low statistical uncertainties since the computation of intradiffusivity is performed using a larger number of solute molecules.

In this work, all diffusivities are corrected for finite-size effects using the Yeh−Hummer equation[82−84]

$$D_i^{\infty} = D_i + \frac{k_B T \xi}{6\pi\eta L} \tag{4}$$

where D_i^{∞} is the finite-size corrected self- (and intra-) diffusion coefficients, T is the absolute temperature, ξ is a dimensionless constant equal to 2.837298, and L is the length of the simulation box. The computation of η does not depend on the system size.[85,86] As recently shown by Jamali et al.,[84,87] eq 4 is valid for correcting the intradiffusion coefficients in binary and multicomponent mixtures. As can be seen in Figure S2, eq 4 can be used to correct the intradiffusivities of infinitely diluted H_2 in liquid (Figure S2a), vapor (Figure S2b), and supercritical (Figure S2c) H_2O computed in MD simulations. In all cases, D_i computed using different numbers of H_2O molecules (solvent) scale linearly with $1/L$ (where $L \propto N^{1/3}$ and N is the number of molecules). The magnitude of the finite-size correction strongly depends on the system and thermodynamic conditions.[36,82,86−89] For example, in the liquid phase (Figure S2a), the absolute deviation between D_i and D_i^{∞} is 3.5, 4.4, and 5.3% for MD simulations using 1000, 2000, and 4000 H_2O

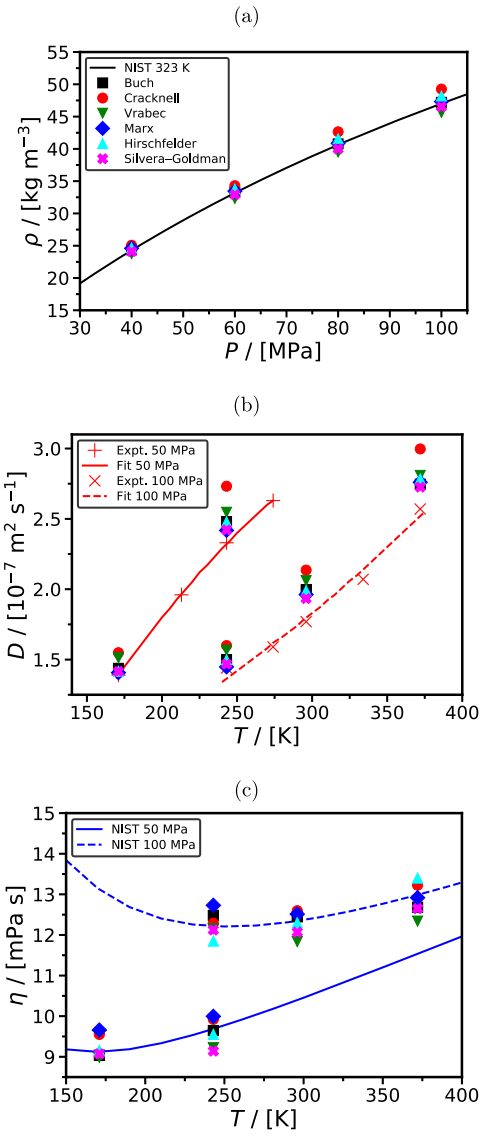

Figure 1. Properties of pure H_2: (a) density as a function of pressure at 323 K, (b) self-diffusion coefficient, and (c) shear viscosity as a function of temperature at 50 and 100 MPa computed in MD simulations using the Buch,[38] Cracknell,[41] Vrabec,[39] Marx,[43] Hirschfelder,[40] and Silvera−Goldman[42] H_2 force fields. The experimental data are taken from the NIST database[90] and Chen et al.[91] The self-diffusion coefficients are corrected for system-size effects using eq 4. The error bars have been omitted for clarity. The raw MD data along with the error bars are listed in Tables 2 and S4 in the Supporting Information. The symbols denoting the different force fields are the same in (a)−(c).

https://doi.org/10.1021/acs.jced.1c00300
J. Chem. Eng. Data 2021, 66, 3226−3244

Table 2. Self-Diffusion Coefficients, Shear Viscosities, and Densities of Pure H_2 Computed Using Different Force Fields for Various Temperatures and Pressures[a]

		Buch		Cracknell		Vrabec		Hirschfelder		Marx		Silvera−Goldman		NIST
T	P	D	σ_D	D	σ_D	D	σ_D	D	σ_D	D	σ_D	D	σ_D	
171	50	1.44	0.03	1.55	0.03	1.51	0.03	1.42	0.03	1.41	0.02	1.42	0.02	
243	50	2.48	0.04	2.73	0.04	2.55	0.04	2.48	0.04	2.42	0.02	2.42	0.02	
243	100	1.50	0.03	1.60	0.04	1.57	0.04	1.50	0.04	1.45	0.03	1.47	0.03	
296	100	2.00	0.04	2.14	0.04	2.06	0.04	1.99	0.04	1.96	0.02	1.93	0.02	
372	100	2.75	0.03	3.00	0.05	2.81	0.05	2.78	0.05	2.76	0.02	2.73	0.02	
		η	σ_η	η	σ_η	η	σ_η	η	σ_η	η	σ_η	η	σ_η	η
171	50	9.04	0.84	9.55	1.02	9.0	0.7	9.16	1.01	9.7	1.3	9.1	0.5	9.121
243	50	9.65	0.55	9.92	1.04	9.2	0.7	9.55	0.81	10.0	1.5	9.1	0.8	9.686
243	100	12.48	0.67	12.3	1.1	12.2	1.3	11.19	0.99	12.7	1.5	12.1	1.0	12.215
296	100	12.45	0.59	12.60	0.91	11.8	1.1	12.3	1.2	12.5	1.6	11.1	1.1	12.344
372	100	12.68	0.37	13.2	1.6	12.3	0.9	13.4	1.3	12.9	0.9	12.0	1.8	12.987
		ρ	σ_ρ	ρ	σ_ρ	ρ	σ_ρ	ρ	σ_ρ	ρ	σ_ρ	ρ	σ_ρ	ρ
323	40	24.4	0.1	25.08	0.08	23.77	0.06	24.68	0.09	24.6	0.2	24.10	0.08	24.547
323	60	33.28	0.09	34.3	0.2	32.32	0.12	33.8	0.2	33.45	0.23	32.91	0.11	33.495
323	80	40.78	0.23	42.65	0.07	39.51	0.09	41.57	0.08	40.87	0.36	39.99	0.23	40.992
323	100	47.21	0.28	49.27	0.06	45.65	0.22	48.18	0.21	47.33	0.13	46.53	0.12	47.210

[a]T is in units of K, P in MPa, D in 10^{-9} m^2 s^{-1}, η in mPa·s, and ρ in kg m^{-3}. σ_x is the uncertainty of quantity x (95% confidence interval of the standard deviation). The values from NIST[90] are shown for comparison.

Table 3. Self-Diffusion Coefficients and Shear Viscosities of Pure O_2 Computed Using Different Force Fields for Various Temperatures and Pressures[a]

		Bohn		Miyano		Coon		NIST
T	P	D	σ_D	D	σ_D	D	σ_D	
77.65	0.1	0.0016	0.0002	0.0022	0.0002	0.0020	0.0002	
194.65	0.1	9.47	0.22	9.72	0.47	9.60	0.31	
273.15	0.1	17.63	0.44	18.12	0.58	17.93	0.29	
298.15	0.1	20.81	0.30	21.11	0.60	21.00	0.68	
318	0.1	23.26	0.42	23.59	0.51	23.73	0.29	
353.15	0.1	28.75	0.51	28.67	0.37	28.69	0.38	
		η	σ_η	η	σ_η	η	σ_η	η
77.65	0.1	284	10	303	11	295	11	292.080
94.65	0.1	13.6	1.6	14.0	1.1	13.8	0.7	14.308
273.15	0.1	16.5	2.0	17.2	2.0	16.9	1.3	19.055
298.15	0.1	17.0	1.7	18.0	1.9	17.7	1.0	20.459
318	0.1	19.8	2.1	20.9	2.1	20.6	2.2	21.542
353.15	0.1	20.8	2.0	21.9	1.7	21.7	2.0	23.394

[a]T is in units of K, P in MPa, D in 10^{-9} m^2 s^{-1}, and η in mPa·s. σ_x is the uncertainty of quantity x (95% confidence interval of the standard deviation). D and η at 77.65 K and 0.1 MPa for the Hansen force field is (0.00248 ± 0.00012) 10^{-9} m^2 s^{-1} and 295 ± 13 mPa·s, respectively. The values from NIST[90] are shown for comparison.

molecules, respectively. In the supercritical and vapor phases, the deviations between D_i and D_i^∞ are found to be one and two orders of magnitude lower, respectively. In this study, the vast majority of diffusivities computed at the supercritical and vapor conditions require finite-size corrections smaller than the uncertainties of the simulations.

For clarity, in the remainder of this manuscript (and the Supporting Information), the symbol D is used for representing the finite-size corrected diffusivities. The uncertainties of the reported densities, shear viscosities, and diffusivities are calculated as standard deviations from at least five independent runs, each one starting from a different initial configuration. The confidence level of all reported uncertainties in this work is 95%.

3. RESULTS AND DISCUSSION

3.1. Force Field Validation and Selection. The following procedure is adopted for selecting accurate force fields to be used for the computation of the intradiffusivities of H_2 and O_2 in H_2O. The six H_2 and six O_2 force fields, described in Section 2.1, are evaluated based on their performance in predicting the density, self-diffusion coefficient, and shear viscosity of the pure gas and the intradiffusion coefficient of the gas in H_2O at low pressures. These properties and conditions are chosen because these force fields are primarily fitted to pure gas experimental data. For more details on the force field parametrization procedure, the reader is referred to the original studies, i.e., for H_2[38−43] and O_2.[53−58] Selected typical comparisons with the available experimental data are shown in Figures 1−4. All of the MD data with the corresponding uncertainties are provided in Table 2 (density, self-diffusion coefficient, and shear viscosity of pure H_2), Table

https://doi.org/10.1021/acs.jced.1c00300
J. Chem. Eng. Data 2021, 66, 3226−3244

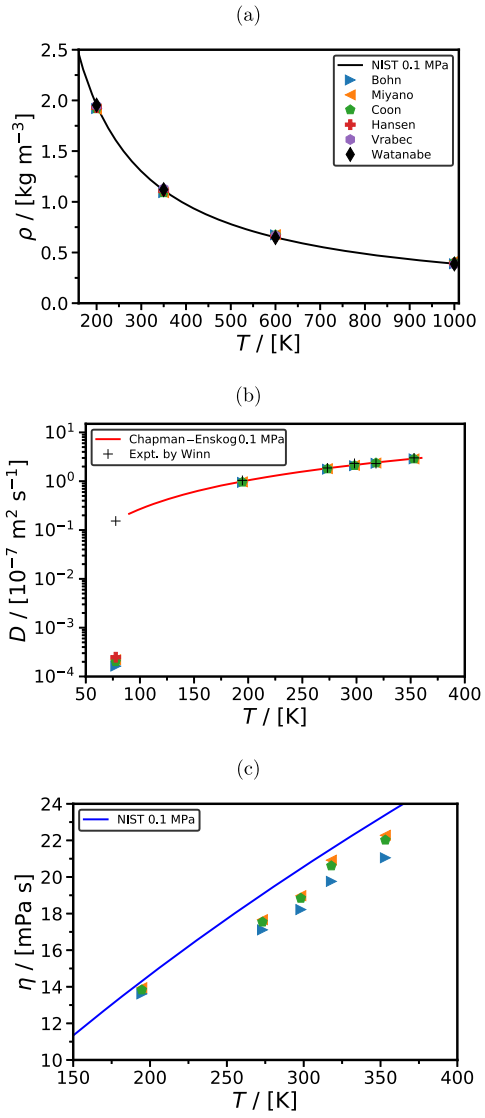

Figure 2. Properties of pure O_2: (a) density, (b) self-diffusion coefficient, and (c) shear viscosity as a function of temperature at 0.1 MPa computed in MD simulations using the Bohn,[53] Miyano,[54] Coon,[55] Hansen,[56] Vrabec,[57] and Watanabe[58] O_2 force fields. The experimental data are taken from the NIST database[90] and Winn.[92] The self-diffusion coefficients are corrected for system-size effects using eq 4. The error bars have been omitted for clarity. The raw MD data along with the error bars are listed in Tables 3 and S5 in the Supporting Information. The symbols denoting the different force fields are the same in (a)−(c).

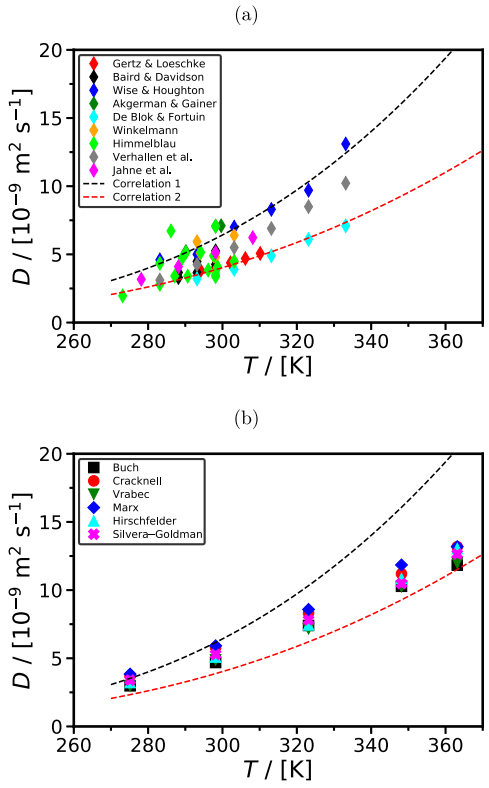

Figure 3. Intradiffusion coefficients of H_2 in H_2O as a function of temperature at 0.1 MPa from (a) experiments, and (b) MD simulations using the Buch,[38] Cracknell,[41] Vrabec,[39] Marx,[43] Hirschfelder,[40] and Silvera−Goldman[42] H_2 force fields combined with the TIP4P/2005 H_2O[35] force field. The experimental data are taken from Gertz and Loeschcke,[94] Baird and Davidson,[95] Wise and Houghton,[96] Akgerman and Gainer,[97] de Blok and Fortuin,[98] Winkelmann,[93] Himmelblau,[9] Verhallen et al.,[99] and Jahne et al.[1] Correlations 1 and 2 are fits to the experimental data using eq 5 (the parameters of the fits are listed in Table 4). The computed intradiffusion coefficients are corrected for system-size effects using eq 4. The error bars have been omitted for clarity. The raw MD data along with the error bars are listed in Table 5.

Table 4. Parameters of the Arrhenius Fit (equation 5) to the Experimental Data of H_2 in H_2O at 1 Atm[a]

	$\ln(D_o)$	α
correlation 1	−12.22 ± 0.48	(−0.199 ± 0.014) × 10^4
correlation 2	−13.29 ± 0.37	(−0.181 ± 0.011) × 10^4

[a]The curves representing the correlations are shown in Figure 3a.

3 (self-diffusion coefficient and shear viscosity of pure O_2), as well as Table S4 (density of pure H_2) and Table S5 (density of pure O_2) in the Supporting Information.

Figure 1 shows the comparison of the computed densities (Figure 1a), self-diffusivities (Figure 1b), and shear viscosities (Figure 1c) of pure H_2 with the available experimental data.[90,91] The respective comparisons with the available experimental data[90,92] for pure O_2 are shown in Figure 2. As shown in Figure 1a, in Table 2 and Table S4 in the Supporting Information, five of the H_2 force fields can accurately predict the density (within 2.5% absolute deviation) at high temperatures and low pressure, while the Cracknell[41] force field deviates from experiments by ca. 8%. At low temperatures and high pressures, four of the H_2 force fields can accurately predict the density (within 2.3% absolute deviation), while for the case of Hirschfelder[40] and Cracknell[41] force fields, the absolute deviation is within 7.5%. For pure O_2, as shown in Figure 2a and in the additional data provided in the Supporting Information (Table S5), four force fields show high accuracy under all conditions studied (absolute average deviations from the experimental data up to 1.5%), while for the case of Miyano[54] and Coon[55] force fields, the absolute average deviation is within 2.4−3.0%. Based on their overall performance in reproducing the experimental density in the temperature range of 200−1000 K, at pressures of 0.1 and 50 MPa (see Table S5 in the Supporting Information), only the force fields by Bohn,[53] Miyano,[54] and Coon[55] are further considered in this study. Nevertheless, the difference in the performance of

https://doi.org/10.1021/acs.jced.1c00300
J. Chem. Eng. Data 2021, 66, 3226−3244

Table 5. Intradiffusion coefficients of H_2 in H_2O and O_2 in H_2O computed using different force field combinations for various temperatures at a pressure of 0.1 MPa[a]

		H_2 in H_2O		O_2 in H_2O	
T	P	D	σ_D	D	σ_D
		Buch + TIP4P/2005		Bohn + TIP4P/2005	
275.15	0.1	3.0	0.3	1.5	0.1
298.15	0.1	4.7	0.7	2.6	0.2
323.15	0.1	7.4	0.5	4.16	0.22
348.15	0.1	10.3	1.5	6.09	0.27
363.15	0.1	11.8	1.1	7.39	0.43
		Cracknell + TIP4P/2005		Miyano + TIP4P/2005	
275.15	0.1	3.70	0.35	1.60	0.12
298.15	0.1	5.80	0.54	2.78	0.11
323.15	0.1	8.3	0.6	4.42	0.26
348.15	0.1	11.20	0.94	6.2	0.3
363.15	0.1	13.18	0.99	7.47	0.47
		Vrabec + TIP4P/2005		Coon + TIP4P/2005	
275.15	0.1	2.97	0.26	1.58	0.11
298.15	0.1	4.9	0.3	2.73	0.18
323.15	0.1	7.16	0.46	4.3	0.2
348.15	0.1	10.25	0.43	6.23	0.29
363.15	0.1	12.0	0.6	7.3	0.3
		Hirschfelder + TIP4P/2005		Hansen + TIP4P/2005	
275.15	0.1	3.22	0.16	1.89	0.11
298.15	0.1	5.09	0.46	3.41	0.21
323.15	0.1	7.45	0.46	5.07	0.38
348.15	0.1	10.84	0.37	6.87	0.28
363.15	0.1	13.05	0.71	7.94	0.29
		Marx + TIP4P/2005		Vrabec + TIP4P/2005	
275.15	0.1	3.8	0.2	2.0	0.1
298.15	0.1	5.9	1.8	3.29	0.11
323.15	0.1	8.6	0.8	4.89	0.23
348.15	0.1	12	1	6.6	0.3
363.15	0.1	13.2	1.8	7.84	0.29
		Silvera−Goldman + TIP4P/2005		Watanabe + TIP4P/2005	
275.15	0.1	3.40	0.81	2.01	0.12
298.15	0.1	5.28	0.79	3.34	0.22
323.15	0.1	7.81	0.76	4.4	0.3
348.15	0.1	10.48	0.69	7.01	0.36
363.15	0.1	12.65	0.79	8.49	0.36

[a] T is in units of K, P in MPa, and D in 10^{-9} m^2 s^{-1}. σ_x is the uncertainty of quantity x (95% confidence interval of the standard deviation).

the chosen force fields with the ones by Hansen,[56] Vrabec,[57] and Watanabe[58] is not very significant.

For the case of H_2 self-diffusion coefficients, we compare the computed data with the experimental data reported by Chen et al.[91] at 50 and 100 MPa. It can be clearly seen in Figure 1b (also in Table 2) that the three-site models perform significantly better than the rest. Particularly, the Silvera−Goldman-type[42] force field has the highest accuracy (absolute average deviation from the experimental data equal to 4.6%), followed by the Marx[43] force field (deviation of 4.8%). Among the single and two-site force fields, the Buch[38] force field shows an accuracy comparable to the three-site models (6.7%). The force fields show mutual consistency for the majority of temperatures and pressures, with the Silver-Goldman[42] being the most accurate and Cracknell[41] being the least accurate. For

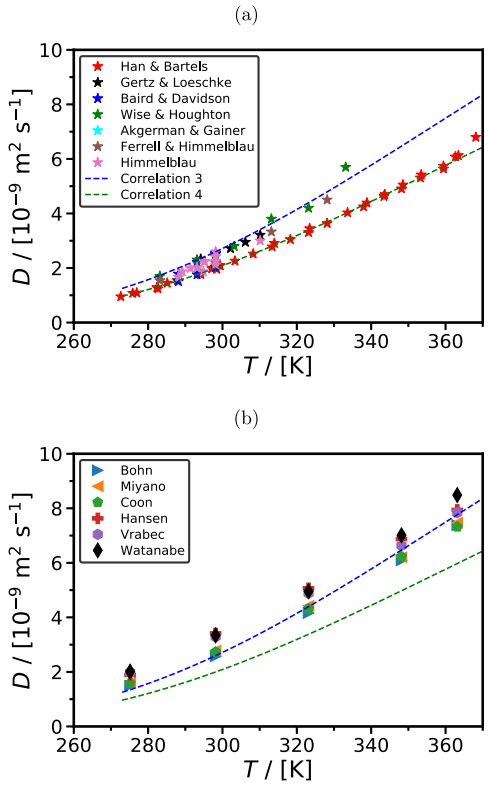

Figure 4. Intradiffusion coefficients of O_2 in H_2O as a function of temperature at 0.1 MPa from (a) experiments, and (b) MD simulations using the Bohn,[53] Miyano,[54] and Coon,[55] Hansen,[56] Vrabec,[57] and Watanabe[58] O_2 force fields combined with the TIP4P/2005 H_2O[35] force field. The experimental data are taken from Han and Bartels,[101] Gertz and Loeschcke,[94] Baird and Davidson,[95] Wise and Houghton,[96] Akgerman and Gainer,[97] Ferrell and Himmelblau,[100] and Himmelblau.[9] Correlation 4 is a fit to experimental data provided by Han and Bartels.[101] Correlation 3 is a 25% positive shift of correlation 4. The computed intradiffusion coefficients are corrected for system-size effects using eq 4. The error bars have been omitted for clarity. The raw MD data along with the error bars are listed in Table 5.

the case of O_2 self-diffusion coefficients in the vapor phase, shown in Figure 2b (also in Table 3), the two-site force fields (i.e., Bohn,[53] Miyano,[54] and Coon[55]) are in excellent agreement with the experimental measurements at 0.1 MPa reported by Winn.[92] In particular, the absolute average deviations are 6.1, 5.2, and 5.8% for the Bohn,[53] Miyano,[54] and Coon[55] force fields, respectively. In sharp contrast, a strong deviation is observed at 77.65 K, where the experimental point has a "vapor-like" value, while the MD simulations predict "liquid-like" values for the self-diffusion coefficient. It should also be noted that according to NIST,[90] the corresponding vapor−liquid−equilibrium (VLE) temperature for 0.1 MPa is ca. 90 K. Therefore, the reported experimental value at 77.65 K may be questionable. The self-diffusivities computed with MD are compared with calculations using the Chapman−Enskog[13] theory for the vapor phase. An almost perfect agreement is found, as can be clearly seen in Figure 2b.

The computed shear viscosities of pure H_2 and O_2 are compared with the values reported by NIST.[90] As shown in Figure 1c, the Buch[38] force field has the best performance (absolute average deviation of 1.3%) in predicting the shear viscosity of pure H_2, clearly reproducing the trend of the NIST

https://doi.org/10.1021/acs.jced.1c00300
J. Chem. Eng. Data 2021, 66, 3226−3244

Table 6. Comparison of the Intradiffusivities of O_2 in H_2O (TIP4P/2005 Force Field) Computed Using Different Force Fields with the Available Experimental Data for Various Temperatures and Pressures[a]

T	P	D	σ_D
		Bohn + TIP4P/2005	
293.15	1.0	2.29	0.16
308.15	1.0	3.04	0.11
283.15	2.5	1.82	0.17
298.15	2.0	2.62	0.12
		Coon + TIP4P/2005	
293.15	1.0	2.32	0.13
308.15	1.0	3.16	0.13
283.15	2.5	1.82	0.13
298.15	2.0	2.41	0.13
		Miyano + TIP4P/2005	
293.15	1.0	2.43	0.12
308.15	1.0	3.32	0.12
283.15	2.5	1.87	0.12
298.15	2.0	2.67	0.12

[a] T is in units of K, P in MPa, and D in 10^{-9} m^2 s^{-1}. σ_x is the uncertainty of quantity x (95% confidence interval of the standard deviation). The intradiffusion coefficients are corrected for system-size effects using eq 4.

shear viscosity dataset. As shown in Figure 2c, the two-site O_2 force fields are relatively accurate in reproducing the shear viscosity reported by NIST.[90] Namely, the absolute average deviations are 9.6, 6.3, and 6.7% for the cases of Bohn,[53] Miyano,[54] and Coon[55] force fields, respectively.

In Figure 3a, we show all of the available experimental values for the H_2 intradiffusion coefficients in H_2O as a function of temperature at 0.1 MPa. For more details on the experiments, the reader is referred to the review papers by Himmelblau[9] and Winkelmann.[93] Additional experimental data for H_2 intradiffusivity in H_2O have been reported by Gertz and Loeschcke,[94] Baird and Davidson,[95] Wise and Houghton,[96] Akgerman and Gainer,[97] de Blok and Fortuin,[98] Verhallen et al.,[99] and Jähne et al.[1] As can be seen in Figure 3a, the majority of the experimental data fall onto two distinct, experimentally based, Arrhenius-type curves (noted as correlations 1 and 2), with some experimental data falling in-between the two curves. The two curves differ by approximately 70%. The Arrhenius-type curves are described as follows:[10,15]

$$D = D_o \exp\left(\frac{\alpha}{T}\right) \tag{5}$$

where D_o and α are the fitting parameters. Often, α is expressed as $\alpha = \frac{-E_a}{R}$, where E_a is the activation energy for diffusion and R is the universal gas constant. The values of the parameters for the two curves are listed in Table 4.

Figure 3b and Table 5 show the MD results for the H_2 intradiffusivities in H_2O at 0.1 MPa as a function of temperature along with correlations 1 and 2. As can be clearly seen, the MD results lie closer to the lower curve (correlation 2), especially for temperatures higher than 310 K. This finding indicates that the experimental data falling onto correlation 1 probably need to be re-evaluated. Among all force field combinations considered for the system H_2−H_2O, the Buch−TIP4P/2005 combination shows the least deviation from correlation 2 for all temperature points (absolute average deviation of 16.4%), followed by the Vrabec—TIP4P/2005 combination (16.6%), while the absolute average deviation for the remaining four combinations is in the range 24−40%.

A similar procedure is followed for the case of O_2 diffusing in H_2O. Himmelblau[9] presented an earlier review, while additional experimental data have been reported by Gertz and Loeschcke,[94] Baird and Davidson,[95] Wise and Houghton,[96] Ferrell and Himmelblau,[100] Akgerman and Gainer,[97] and Han and Bartels.[101] Figure 4a shows all of the available experimentally measured O_2 intradiffusion coefficients in H_2O as a function of temperature at 0.1 MPa. Similar to the H_2−H_2O system, the majority of the experimental data fall onto two distinct curves (noted as correlations 3 and 4 in Figure 4), with some data falling in-between the two curves. The two curves differ by approximately 25%. The experimental study by Han and Bartels[101] is by far the most extensive for the O_2 intradiffusivity in H_2O spanning temperatures up to 370 K. The data points reported in this study are in excellent agreement with correlation 4, as clearly seen in Figure 4a. Our MD results for the O_2 intradiffusivities in H_2O at 0.1 MPa, along with the two correlations, are shown as a function of temperature in Figure 4b and listed in Table 5. It is evident that the computed intradiffusion coefficients, regardless of the force field used, are in very good agreement with correlation 3, while they systematically deviate from the experimental data reported by Han and Bartels,[101] and therefore, correlation 4. Based on this finding, for the remainder of the study, the experimental data falling onto correlation 3 are adopted. The combination of our MD results with the rest of the experiments suggests that the experimental data of Han and Bartels[101] probably need to be revisited. Among the six force field combinations considered for the system O_2−H_2O, the Bohn−TIP4P/2005 combination showed the highest agreement with the adopted correlation of experimental values (absolute average deviation of 3.8%), followed by the Coon−TIP4P/2005 combination (6.4%), and the Miyano−TIP4P/2005 combination (7.4%), while the absolute average deviation of the remaining three combinations ranged from 17.6 to 20.1%. The good performance of this force field combination is further confirmed by additional MD simulations of O_2 diffusing in H_2O, performed at higher pressures, i.e., 1.0, 2.0, and 2.5 MPa, for which the experimental data are available.[102] These results are shown in Table 6.

Based on our findings for the pure gas (H_2 and O_2) properties and for the gas diffusion in H_2O, we conclude that the Buch−TIP4P/2005 force field combination is the most suitable for modeling H_2 intradiffusion in H_2O, and the Bohn−TIP4P/2005 force field combination is the most suitable for modeling O_2 intradiffusion in H_2O. Therefore, all of the remaining simulations are performed with these two combinations.

3.2. Engineering a Model for Predicting the Intradiffusivities of H_2 and O_2 in H_2O. In this work, extensive MD simulations have been performed for the computation of the intradiffusivities of H_2 and O_2 in H_2O at temperatures in the range 275.15−975.15 K and pressures 0.1−200 MPa. In our simulations, the self-diffusion coefficients of pure H_2O are also computed for the same wide T and P range. All of the results are listed in Tables 7, 8, and 9 for the intradiffusivity of H_2 in H_2O, O_2 in H_2O, and the self-diffusivity of pure H_2O, respectively. Figure 5a shows an Arrhenius-type plot of the computed intradiffusion coefficients for the H_2−H_2O system. The respective results for the O_2−H_2O and pure H_2O systems

https://doi.org/10.1021/acs.jced.1c00300
J. Chem. Eng. Data 2021, 66, 3226−3244

Table 7. Intradiffusion Coefficients of H_2 in H_2O Computed for a Wide Range of Temperatures and Pressures[a]

	D	σ_D	D	σ_D	D	σ_D	D	σ_D	D	σ_D	D	σ_D	D	σ_D	D	σ_D	D	σ_D
T/P	0.1		5.0		7.5		10		12.5		20		30		100		200	
275.15	2.98	0.31	2.99	0.18			3.02	0.24			3.11	0.23	2.98	0.18				
298.15	4.69	0.74	4.86	0.37			4.92	0.34			4.87	0.19	4.85	0.28	4.26	0.24	3.80	0.17
323.15	7.41	0.49	7.48	0.58			7.24	0.25			7.14	0.54	6.90	0.65				
348.15	10.3	1.5	10.28	0.66			10.70	0.42			10.27	0.72	10.17	0.99				
363.15	11.8	1.1	12.09	0.41			12.57	0.48			11.90	0.52	11.73	0.92	10.79	0.78	9.18	0.42
423.15															17.9	2.1	15.7	2.0
448.15			24.5	1.2			24.8	1.1			24.89	0.83	25.8	1.4				
473.15															29.9	1.8	27.3	1.8
498.15			38.6	2.0			35.3	3.4			35.6	2.7	35.5	2.4				
523.15					44.5	5.4									34.2	1.8	29.9	1.8
573.15			5125	670	2470	231	66.5	4.3	63.9	1.9	60.8	3.4	59.2	3.5				
586.15							1967.9	151.3										
623.15							2559.0	202.4	1871	286			90.4	5.1	60.9	2.4	47.9	2.1
637.15											147	11	103.1	9.1				
641.15											774	23						
657.15													148	10	72.2	2.5		
673.15			7400	767	4554	389	3212	223	2421	192	1211	68	262	17	80.8	3.6		
723.15											1624	123	814	68	105.5	4.9		
773.15			9260	1259	5881	466	4088	327	3376	293	2000	202	1148	109	149.0	8.4		
823.15													1377	121	205.7	9.2		
873.15			11 196	1599	7329	551	5098	389	4155	277	2562	189	1667	144	274	16		
973.15			14 295	1918	9328	721	6616	403	5066	281	3161	220	1988	227	432	19		

[a]The Buch[38] and TIP4P/2005[35] force fields are used for H_2 and H_2O, respectively. T is in units of K, P in MPa, and D in 10^{-9} m^2 s^{-1}. σ_x is the uncertainty of quantity x (95% confidence interval of the standard deviation).

https://doi.org/10.1021/acs.jced.1c00300
J. Chem. Eng. Data 2021, 66, 3226−3244

Table 8. Intradiffusion Coefficients of O_2 in H_2O Computed for a Wide Range of Temperatures and Pressures[a]

	D	σ_D	D	σ_D	D	σ_D	D	σ_D	D	σ_D	D	σ_D	D	σ_D	D	σ_D	D	σ_D	D	σ_D
T/P	0.1		2.5		5.0		7.5		10		12.5		20		30		100		200	
275.15	1.50	0.10					1.41	0.17												
298.15	2.57	0.20									2.48	0.24	2.49	0.21	2.46	0.19	2.34	0.18	2.22	0.18
323.15	4.16	0.22																		
348.15	6.09	0.27	5.80	0.32					5.79	0.77										
363.15	7.39	0.43											7.03	0.81	6.99	0.80	6.44	0.79	5.83	0.79
423.15									12.4	1.1	12.4	1.3								
448.15							15.0	1.7					15.0	1.9	14.8	1.7	13.3	1.2	12.8	1.5
498.15									21.4	2.5										
523.15													25.5	1.7	24.0	1.6	20.9	1.6	18.1	1.6
573.15							833.9	43.4	36.8	3.2			33.1	3.4	32.8	2.6	27.5	2.9	22.3	2.5
673.15					1842	144			902	29	714	31	381.5	2.5			43.2	2.4	33.5	2.7
723.15							1390	41												
773.15									1219	64	958	95	580	33	374	12	68.5	2.6		
873.15					2853	277	2002	119	1561	74	1179	69	735	61			110.0	9.0		
973.15							2375	116	1796	56	1527	50	903	44	590	36	166	17	83.0	6.4

[a]The Bohn[53] and TIP4P/2005[35] force fields are used for O_2 and H_2O, respectively. T is in units of K, P in MPa, and D in 10^{-9} m^2 s^{-1}. σ_x is the uncertainty of quantity x (95% confidence interval of the standard deviation).

https://doi.org/10.1021/acs.jced.1c00300
J. Chem. Eng. Data 2021, 66, 3226−3244

Table 9. Self-Diffusion Coefficients of Pure H_2O Computed for a Wide Range of Temperatures and Pressures Using the TIP4P/2005 Force Field[a]

	D	σ_D	D	σ_D	D	σ_D	D	σ_D	D	σ_D	D	σ_D	D	σ_D	D	σ_D	D	σ_D
T/P	0.1		5.0		7.5		10		12.5		20		30		100		200	
275.15	1.57	0.02	1.57	0.02			1.56	0.02			1.55	0.02	1.55	0.02				
298.15	2.64	0.05	2.63	0.05			2.62	0.05			2.62	0.04	2.61	0.04	2.58	0.03	2.54	0.03
323.15	4.29	0.05	4.27	0.06			4.23	0.05			4.22	0.06	4.20	0.06				
348.15	6.26	0.07	6.26	0.07			6.24	0.06			6.22	0.07	6.17	0.06				
363.15	7.53	0.07	7.53	0.07			7.52	0.08			7.52	0.08	7.51	0.08	7.30	0.11	6.81	0.72
423.15															12.92	0.15	11.94	0.14
448.15			16.9	1.6			16.9	1.4			16.7	1.5	16.6	1.4				
473.15															18.46	0.17	17.12	0.16
498.15			24.0	2.2			23.9	2.0			23.7	2.1	22.9	1.8				
523.15					28.1	2.4									24.2	2.2	21.35	0.20
573.15			1024	16	458.5	9.8	38.7	3.0	38.4	3.3	37.4	3.3	36.1	3.2				
586.15							432.7	5.2										
623.15							563.4	5.8	409.3	5.0			49.7	3.9	38.8	3.2	32.67	0.21
637.15											65.9	4.8	55.4	4.4				
641.15											178.9	7.4						
657.15													68.5	4.8	45.2	3.5		
673.15			1593	17	972	14	743.1	9.8	569.1	6.9	293.7	6.1	97.1	5.7	48.7	3.9		
723.15											413.8	9.4	231.2	8.6	61.1	4.8		
773.15			2219	27	1466	15	1164	13	875.5	7.6	518.8	8.0	315.6	7.9	76.8	4.8		
823.15													396.0	8.0	97.8	5.7		
873.15			2867	27	1918	23	1481	18	1211.6	8.3	733.0	8.0	472.7	7.1	122.3	6.1		
973.15			3486	29	2385	24	1879	20	1536.1	9.7	955	9	630.4	5.1	176.0	6.2		

[a] T is in units of K, P in MPa, and D in 10^{-9} m^2 s^{-1}. σ_x is the uncertainty of quantity x (95% confidence interval of the standard deviation).

https://doi.org/10.1021/acs.jced.1c00300
J. Chem. Eng. Data 2021, 66, 3226−3244

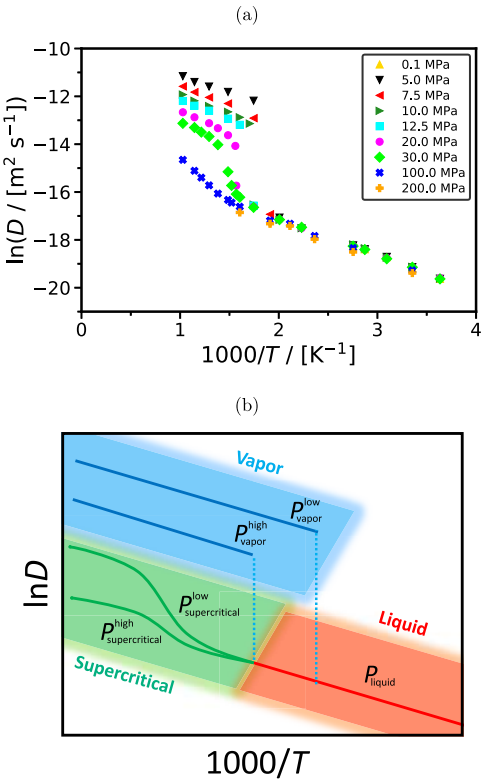

Figure 5. (a) Arrhenius-type plot of the computed intradiffusion coefficients of H_2 in H_2O using the Buch[38]−TIP4P/2005[35] force field combination. The respective results for the O_2−H_2O and pure H_2O systems are shown in Figure S3a,b, and Tables 8 and 9, respectively. The computed intradiffusion coefficients are corrected for system-size effects using eq 4. The error bars have been omitted for clarity. All raw MD data shown here along with the error bars are listed in Table 7. (b) A conceptual schematic representation of the diffusivity patterns of the H_2 in H_2O, O_2 in H_2O, and pure H_2O systems in the vapor, liquid, and supercritical regions.

are shown in Figure S3a,b, respectively, in the Supporting Information. All systems exhibit similar patterns in their Arrhenius plots. A conceptual schematic representation of these patterns is shown in Figure 5b. Since our MD simulations span a wide T and P range, the gas−H_2O systems can be in the vapor, liquid, or supercritical state. We assume that the critical point and the VLE properties are the same as those of the pure H_2O since H_2 and O_2 are present at infinite dilution in the aqueous phase. According to Wagner and Pruss,[103] the critical temperature T_c and pressure P_c of H_2O are 647.096 K and 22.064 MPa, respectively. According to Vega and Abascal,[59] the T_c and P_c of the TIP4P/2005 H_2O force field are 640 K and 14.6 MPa, respectively. Our analysis, therefore, is based on the critical point of the TIP4P/2005 H_2O force field. Three distinct zones can be identified in Figure 5b, based on whether the diffusion occurs in the vapor, liquid, or supercritical phase. Each zone has specific characteristics. In particular, the vapor and the liquid zones exhibit Arrhenius behavior as described by eq 5. As can be seen in Figure 5, the slopes of the vapor and liquid zones in the $\ln(D)$ vs $1000/T$ plot have very similar values. A very weak pressure dependence is observed for the case of the liquid zone (Figure 5a), while a strong pressure dependence is observed in the vapor zone. The supercritical zone exhibits a more complex non-Arrhenius behavior. Yet, narrow temperature ranges could be identified where an Arrhenius behavior is locally present. These characteristics enable us to develop a systematic and generalizable approach for the estimation of the intradiffusion coefficients at the three different zones. To establish the new approach, we examine the gas diffusion in the three zones (i.e., vapor, liquid, and supercritical) separately. Figure 6 shows the overall diffusion behavior of the three systems examined. Namely, the intradiffusion coefficients of H_2 in H_2O, as a function of the inverse temperature, in the vapor (Figure 6a), liquid (Figure 6d), and supercritical (Figure 6g) phases. The respective intradiffusivities of O_2 in H_2O are shown in Figures 6b,e,h. Finally, the respective self-diffusivities for pure H_2O are shown in Figure 6c,f,i.

It should be noted that the experimentally measured solubilities of H_2 and O_2 in H_2O are rather low in the entire range of temperatures and pressures examined in this work.[104−107] For pressures close to the atmospheric and temperatures up to 353 K, the solubility of H_2 in H_2O ranges from 1.3×10^{-5} to 4×10^{-4}. For pressures up to ca. 60 MPa and temperatures up to 373 K, the solubilities increase by an order of magnitude. For higher temperatures and very high pressures, e.g., 100 MPa, the solubilities increase to a maximum of approximately 1×10^{-2}.[106] The solubilities of O_2 in H_2O are in the same range.[107] For high pressures, where the solubility values of the gases in H_2O are significantly higher than in the infinite dilution limit, the computation of mutual diffusivities (Fick and Maxwell-Stefan[10,11]) would be of practical interest since the mass transport occurs due to gradients in composition (or chemical potential). To this purpose, one can either use Darken equation-based models[14] or can follow the well-established methodology of computing the Maxwell-Stefan diffusivities ($Đ_{MS}$) from the Onsager coefficients in MD simulations,[20,71,84] and the thermodynamic factor (Γ), e.g., from Kirkwood−Buff integrals.[108,109] Fick diffusivities follow from $D_{Fick} = \Gamma\, Đ_{MS}$.[10,20,71,80] Such an approach is outside the scope of the current work, which is to construct an engineering model for predicting the diffusivities of infinite diluted gases in H_2O (for which $D_{self} = Đ_{MS} = D_{Fick}$[10]).

3.2.1. Gas Diffusivity in H_2O Vapor. MD simulations are performed for four different isobars (i.e., 5.0, 7.5, 10.0, and 12.5 MPa) and various temperatures that correspond to H_2O (TIP4P/2005 force field) being in the vapor phase. From the Arrhenius plots for H_2 in H_2O (Figure 6a), O_2 in H_2O (Figure 6b), and pure H_2O (Figure 6c), a linear behavior and a strong pressure dependence can be observed. The dotted lines in these figures show the linear fits to each isobar. Thus, a value for the slope (α) and the intercept ($\ln(D_o)$) can be calculated for each one. The values for the slope and intercept are plotted as a function of pressure in Figure 7a,b, respectively, where the following linear behavior is established

$$\alpha = m_1 P + m_0 \tag{6}$$

$$\ln(D_o) = n_1 P + n_0 \tag{7}$$

where m_0, m_1, n_0, and n_1 are fitting parameters. The calculated fitting parameters for the three systems considered in the current study are listed in Table 10. These parameters are an important result since they can be used to calculate the self- and intradiffusion coefficients for any conditions where the solute diffusion occurs in the gaseous phase by combining eqs 5−7 into the following equation

https://doi.org/10.1021/acs.jced.1c00300
J. Chem. Eng. Data 2021, 66, 3226−3244

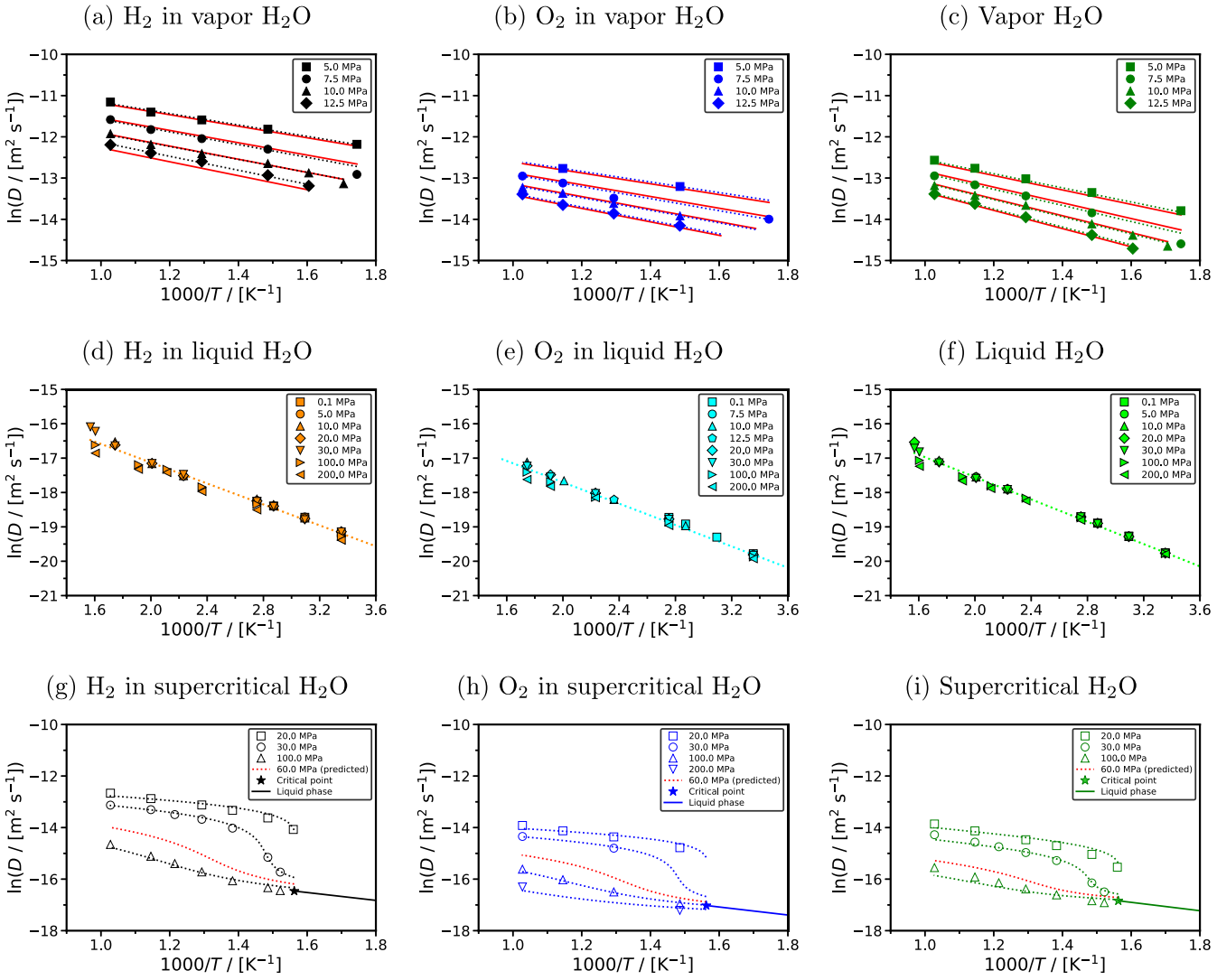

Figure 6. Arrhenius-type plots of the computed intradiffusion coefficients of H_2 in H_2O, O_2 in H_2O, and pure H_2O in the vapor (a–c), liquid (d–f), and supercritical phase (g–i), respectively. The dotted lines in (a)–(c) are pressure specific Arrhenius fits using eq 5. The red solid lines show the generalized fits using eq 8 (the parameters of the fit are listed in Table 10). The dotted lines in (d)–(f) are unified Arrhenius fits using eq 5 (the parameters are listed in Table 11). The dotted lines in (g)–(i) are fits using eq 9 (the parameters are listed in Table 13). The Buch,[38] Bohn,[53] and TIP4P/2005[35] force fields are used for H_2, O_2, and H_2O, respectively. The computed intradiffusion coefficients are corrected for system-size effects using eq 4. Error bars have been omitted for clarity. The raw MD data along with the error bars are listed in Tables 7, 8, and 9.

Table 10. Parameters of the Generalized Equation 8 for Predicting the Diffusivities in the Vapor Phase

	H_2 in H_2O	O_2 in H_2O	pure H_2O
m_0	$(-1.21 \pm 0.06) \times 10^3$	$(-1.10 \pm 0.06) \times 10^3$	$(-1.45 \pm 0.09) \times 10^3$
m_1	$(-0.39 \pm 0.07) \times 10^1$	$(-0.43 \pm 0.07) \times 10^1$	$(-0.61 \pm 0.09) \times 10^1$
n_0	-9.35 ± 0.12	-10.98 ± 0.04	-10.63 ± 0.01
n_1	$(-0.92 \pm 0.13) \times 10^{-2}$	$(-0.63 \pm 0.05) \times 10^{-2}$	$(-0.40 \pm 0.01) \times 10^{-2}$

$$D = \exp\left[(n_1 P + n_0) + (m_1 P + m_0)\frac{1}{T}\right] \quad (8)$$

As can be seen in Figure 6a–c, the MD results and the calculations using eq 8 (solid red lines) are in very good agreement. In particular, eq 8 can fit the MD data with an absolute average deviation of 6.7, 3.9, and 7.1% for the H_2 in H_2O, O_2 in H_2O, and pure H_2O systems, respectively.

3.2.2. Gas Diffusivity in Liquid H_2O. MD simulations are performed for eight different isobars (i.e., 0.1, 5.0, 10.0, 12.5, 20.0, 30.0, 100.0, and 200.0 MPa) and various temperatures that correspond to H_2O (TIP4P/2005 force field) being in the liquid phase. Contrary to the strong pressure dependence that is observed for the case of gas diffusivity in the vapor phase, a weak pressure dependence is observed for the liquid phase. This is expected since liquid H_2O is almost incompressible. As shown in Figure 6d–f, single curves (dotted lines) can fit the MD data in the pressure range of 0.1–200 MPa with an absolute average deviation of 9.3, 9.1, and 7.1% for the cases of H_2 in H_2O, O_2 in H_2O, and pure H_2O, respectively. The corresponding parameters for the Arrhenius fit are shown in Table 11. However, to increase the accuracy of the proposed

https://doi.org/10.1021/acs.jced.1c00300
J. Chem. Eng. Data 2021, 66, 3226–3244

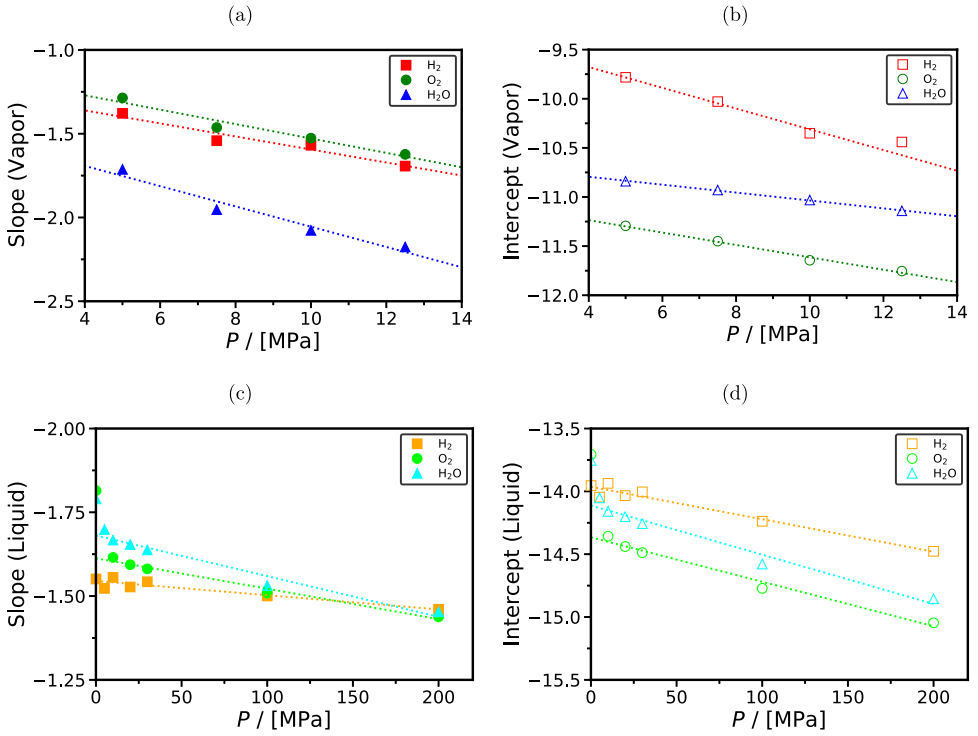

Figure 7. (a) Slopes and (b) intercepts of the linear fits to the MD diffusivity data for the H_2 in H_2O, O_2 in H_2O, and pure H_2O systems in the vapor phase shown in Figure 6a–c as a function of pressure. The dotted lines in (a) and (b) are fits using eqs 6 and 7, respectively (the parameters of the fits are listed in Table 10). The (c) slopes and (d) intercepts of the linear fits to the MD diffusivity data for the H_2 in H_2O, O_2 in H_2O, and pure H_2O systems in the liquid phase shown in Figure 6d–f as a function of pressure. The dotted lines in (c) and (d) are fits using eqs 6 and 7, respectively (the parameters of the fits are listed in Table 12).

Table 11. Parameters of the Unified Arrhenius Fit Equation 5 Using all Diffusivity Data in the Liquid Phase[a]

	$\ln(D_o)$	α
H_2 in H_2O	−14.09 ± 0.08	$(-0.152 \pm 0.003) \times 10^4$
O_2 in H_2O	−14.59 ± 0.08	$(-0.155 \pm 0.003) \times 10^4$
pure H_2O	−14.30 ± 0.06	$(-0.162 \pm 0.002) \times 10^4$

[a]The curves representing the correlations are shown in Figure 6d–f.

methodology, we follow an approach similar to the one used for the vapor phase. A linear fit is performed for each isobar, and subsequently, the calculated slopes and intercepts are expressed as a function of pressure using eqs 6 and 77. The slopes and intercepts are shown in Figure 7c,d, respectively. Table 12 shows the calculated fitting parameters for the three cases considered in the current study. These parameters can be used in eq 8 to calculate the self- and intradiffusion coefficients for any pressure and temperature below the critical point where the solute diffusion occurs in the liquid phase. Equation 8 can fit the MD data with an absolute average deviation of 5.1, 5.6, and 4.6% for the H_2 in H_2O, O_2 in H_2O, and pure H_2O systems, respectively. The resulting absolute average deviations are improved when compared to the case of using a single curve for all pressures.

3.2.3. Gas Diffusivity in Supercritical H_2O. MD simulations are performed for three different isobars (i.e., 20.0, 30.0, and 100.0 MPa) and various temperatures that correspond to H_2O (TIP4P/2005 force field) being in the supercritical phase. As can be observed in Figure 6g–i for the cases of H_2 in H_2O, O_2 in H_2O, and pure H_2O, respectively, the supercritical zone exhibits a more complex, non-Arrhenius behavior. Away from the critical point, Arrhenius behavior can be observed in the temperature range of 675–975 K. Such a behavior has also been reported by a number of studies.[25−27] For example, Zhao et al.[26] reported MD simulations following an Arrhenius behavior at 25 MPa and temperatures in the range of 673–973 K. To generalize the methodology developed here, the computed self- and intradiffusivity data for the supercritical region have been collapsed onto a single curve that has the following form

$$\ln(D) = o_2 (\ln(\rho))^2 + o_1 \ln(\rho) + o_0 \quad (9)$$

where ρ is the density of H_2O (in kg/m^3), while o_0, o_1, and o_2 are fitting parameters. Figure 8 shows the resulting fits, while the calculated parameters for the three cases considered in this

Table 12. Parameters of the Generalized Equation 8 for Predicting the Diffusivities in the Liquid Phase

	H_2 in H_2O	O_2 in H_2O	pure H_2O
m_0	$(-1.55 \pm 0.01) \times 10^3$	$(-1.67 \pm 0.05) \times 10^3$	$(-1.71 \pm 0.02) \times 10^3$
m_1	$(0.42 \pm 0.07) \times 10^{-1}$	0.13 ± 0.05	0.14 ± 0.03
n_0	−13.96 ± 0.02	−14.18 ± 0.15	−14.03 ± 0.07
n_1	$(-0.26 \pm 0.02) \times 10^{-3}$	$(-0.49 \pm 0.16) \times 10^{-3}$	$(-0.45 \pm 0.08) \times 10^{-3}$

https://doi.org/10.1021/acs.jced.1c00300
J. Chem. Eng. Data 2021, 66, 3226−3244

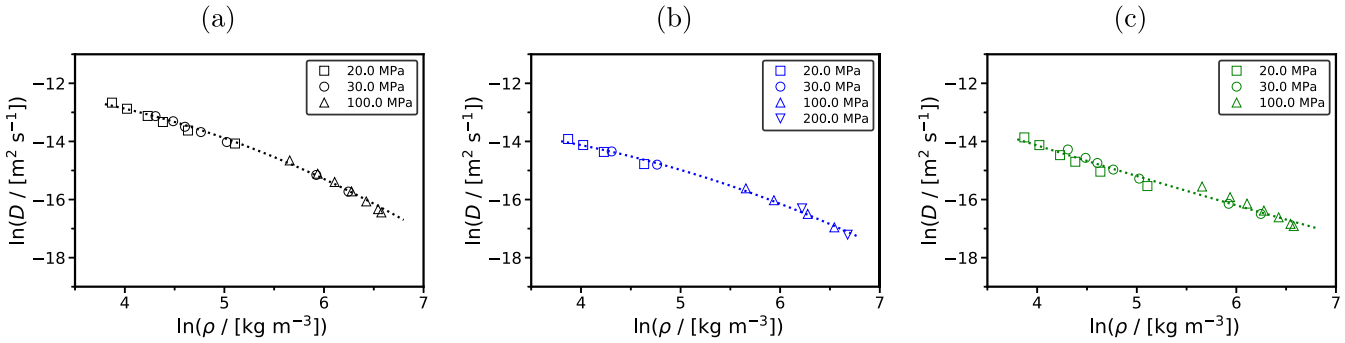

Figure 8. Logarithm of the computed intradiffusivities of (a) H_2 in H_2O, (b) O_2 in H_2O, and (c) pure H_2O in the supercritical region as a function of the logarithm of density. The dotted lines are fits using eq 9 (the parameters for the fits are listed in Table 13). The Buch,[38] Bohn,[53] and TIP4P/2005[35] force fields are used for H_2, O_2, and H_2O, respectively. The computed intradiffusion coefficients are corrected for system-size effects using eq 4. Error bars have been omitted for clarity. All raw MD data shown here along with the error bars are listed in Tables 7, 8, and 9.

Table 13. Parameters of the Generalized Equation 9 for Predicting the Diffusivities in the Supercritical Phase

	H_2 in H_2O	O_2 in H_2O	pure H_2O
o_0	−12.76 ± 0.94	−13.83 ± 1.24	−9.54 ± 1.72
o_1	0.76 ± 0.37	0.55 ± 0.49	−1.23 ± 0.67
o_2	−0.197 ± 0.035	−0.156 ± 0.046	0.02 ± 0.06

study are listed in Table 13. Therefore, eq 9 can be used to calculate the self- and intradiffusion coefficients for any pressure and temperature above the critical point where the solute diffusion occurs in the supercritical phase. Density values can be either from MD simulations or from NIST[90] in case no MD data are available. Equation 9 can fit the MD data with an absolute average deviation of 6.8, 7.1, and 11.3% for the H_2 in H_2O, O_2 in H_2O, and pure H_2O systems, respectively.

3.3. Additional Comparisons with the Literature. The computed densities and shear viscosities of pure H_2O, along with the corresponding uncertainties, are reported in the Supporting Information (Tables S6 and S7 for densities and shear viscosities, respectively). A comparison between the MD values with those reported by NIST[90] can be seen in the Supporting Information in Figure S4a for density and Figure S4b for shear viscosity. The self-diffusivity of H_2O has been extensively discussed in a recent review.[36] The vast majority of the experimental and computational studies discussed in that review are at subcritical conditions (mainly liquid). Therefore, this work provides new data for the pure TIP4P/2005 H_2O in the vapor and supercritical phase. Krynicki et al.[110] reported a correlation for the self-diffusivity of H_2O based on the extensive experimental measurements presented in that work in the temperature range of 275−498 K and for pressures up to 150 MPa. The H_2O self-diffusion coefficients calculated with the generalized expression developed in the current study have an absolute average deviation of 12.7% from the correlation of the experimental data of Krynicki et al.[110] The absolute average deviation drops to 11.1% when the actual MD values are compared instead.

We also compared the H_2O self-diffusion coefficients computed here with other MD studies that used the TIP4P/2005 H_2O force field. Note that the comparison is limited only to studies reporting diffusivities that have been corrected for system-size effects or have been computed in MD simulations of more than 1000 H_2O molecules (following the recommendation in the review paper by Tsimpanogiannis et al.[36]).

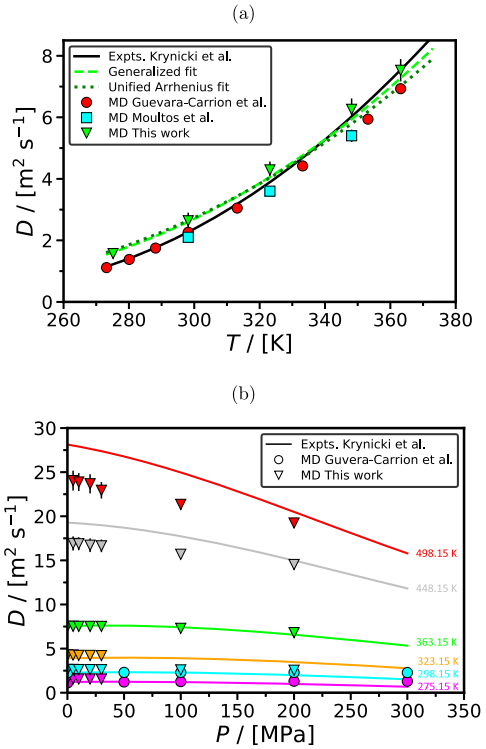

Figure 9. (a) Comparison between the experimentally[110] measured self-diffusivities of pure H_2O at 0.1 MPa with MD simulations performed by Guevara-Carrion et al.,[111] Moultos et al.,[64] and this study using the TIP4P/2005[35] force field. (b) Comparison between the experimentally[110] measured self-diffusivities of pure H_2O at various pressures with MD simulations performed by Guevara-Carrion et al. and in this study using the TIP4P/2005 force field. The self-diffusivities computed in this work have been corrected for system-size effects using eq 4, while the ones reported by Guevara-Carrion et al. and Moultos et al. have been computed in MD simulations using 2000 molecules or more. The generalized fit to the MD data of this study is performed using eq 8 (the parameters of the fit are listed in Table 12). The unified Arrhenius fit to the MD data of this study is performed using eq 5 (the parameters are listed in Table 11).

Figure 9a shows the comparison of the H_2O self-diffusion coefficients for the TIP4P/2005 H_2O force field at 0.1 MPa and temperatures up to 363 K, computed here, with the simulations reported by Guevara-Carrion et al.[111] and Moultos et al.[64] The MD results are also compared with the correlation

https://doi.org/10.1021/acs.jced.1c00300
J. Chem. Eng. Data 2021, 66, 3226−3244

Table 14. Comparison of the Diffusivities Computed in this Work and in Kallikragas et al.[24] Expressed as % Absolute Average Deviation (% AAD), Defined as: $\%\mathrm{AAD} = 100 \times \frac{\sum_{i=1}^{N_{\mathrm{data}}} \left| \frac{D_i^{\mathrm{this\ work}} - D_i^{\mathrm{Kallikragas}}}{D_i^{\mathrm{this\ work}}} \right|}{N_{\mathrm{data}}}$, where N_{data} Denotes the Number of Data Points

phase	system	T range (K)	N_{data}	MD correlation eq 8	MD data
vapor	H_2 in H_2O	>460	21	21.4	22.2
	O_2 in H_2O	>460	14	11.8	11.1
	pure H_2O	>460	21	18.3	17.7
liquid	H_2 in H_2O	>460	14	17.7	4.6
	H_2 in H_2O	all	50	24.2	20.0
	O_2 in H_2O	>460	15	15.3	12.5
	O_2 in H_2O	all	33	19.5	16.2
	pure H_2O	>460	20	16.0	13.6
	pure H_2O	all	51	11.2	12.1
supercritical	H_2 in H_2O	>460	20	12.3	6.3
	O_2 in H_2O	>460	12	15.3	8.8
	pure H_2O	>460	20	13.5	11.0

of the experimental measurements reported by Krynicki et al.[110] Our data deviate from the experimental correlation by 11.8%. Figure 9b shows the comparison of our MD results with the experiments of Krynicki et al. at higher pressures. The minimum deviation from the experimental correlation is 1.4% for the 363.15 K isotherm, while the maximum deviation is 26.9% for the 275.15 K isotherm. The corresponding deviations for the 298.15, 323.15, 448.15, and 498.15 K are, 16.2, 8.1, 10.6, and 13.3%, respectively.

Next, we compared the self-diffusivities computed here with those reported by Kallikragas et al.[24] The authors used the SPCE H_2O force field[112] and performed simulations using 343 molecules. The self-diffusion coefficients have been correlated for temperatures above 460 K. To this purpose, Kallikragas et al. used an equation with 14 parameters based on a formulation by Kawasaki and Oppenheim.[113] Table 14 shows the comparison of our data with the ones reported by Kallikragas et al. for the H_2 diffusivity in H_2O, O_2 in H_2O, and pure H_2O. Considering that the MD simulations of Kallikragas et al. are performed with less than 1000 H_2O molecules, while no system-size corrections have been reported, a shift to higher values of at least 5% should be expected for the reported MD results. This brings our data even closer to the ones by Kallikragas et al. Although the expression by Kallikragas et al. can fit their MD data with an accuracy of ca. 1%, which is higher than the accuracy of the methodology presented here, it requires the fitting of more parameters, i.e., 14 parameters for T > 460 K, while our model has 11 parameters for the temperature range 275.15−975.15 K.

Finally, we report a comparison with MD at supercritical conditions. Figure 10 shows a comparison of our generalized model (eq 8) with MD intradiffusivity data from Zhao et al.[25−27] for the cases of H_2 in H_2O (Figure 10a), O_2 in H_2O (Figure 10b), and pure H_2O (Figure 10c). The intradiffusion coefficients computed in this work are corrected for system-size effects using eq 4, while the ones reported by Zhao et al. have no system-size corrections; however, they have been computed with 4161, 4125, and 900 H_2O molecules for the cases of H_2 in H_2O, O_2 in H_2O, and pure H_2O, respectively. Very good agreement is observed between the correlations of

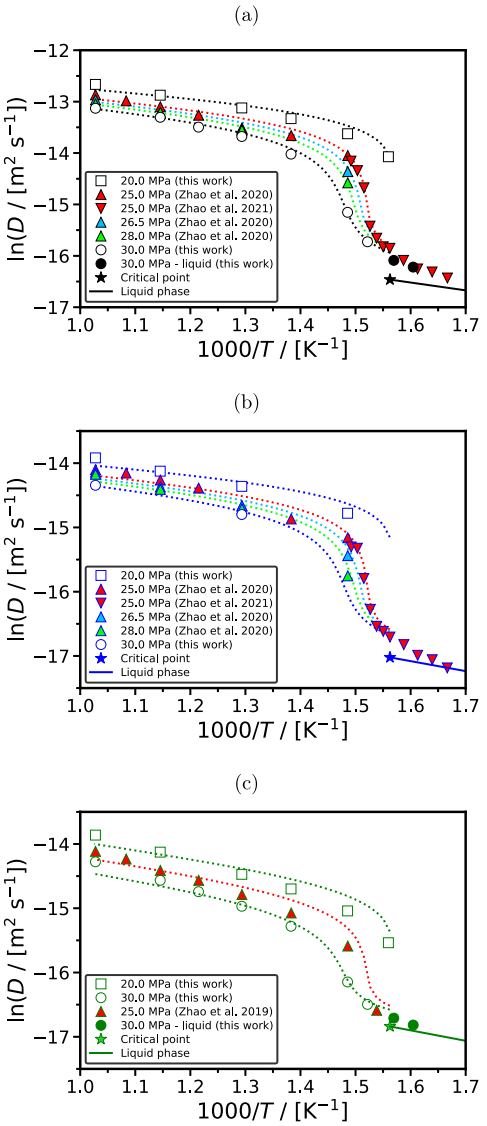

Figure 10. Comparison of our generalized model (eq 8) with MD diffusivity data from Zhao et al.[25−27] for the cases of (a) H_2 in H_2O, (b) O_2 in H_2O, and (c) pure H_2O. The diffusion coefficients computed in this work are corrected for system-size effects using eq 4, while the ones reported by Zhao et al. have been computed using 900−4161 H_2O, 42 H_2, and 24 O_2. Zhao et al. used the TIP4P/2005,[35] Yang and Zhong,[114] and CHARMM[115] force fields for H_2O, H_2, and O_2, respectively. The statistical uncertainties are in the range of 5−10%. The error bars have been omitted for clarity.

our MD simulations (eq 9) and those reported by Zhao et al.[25−27] In particular, the absolute average deviations between the values obtained from eq 9 and those reported by Zhao et al. are 7.2, 9.1, and 12.4% for the cases of diffusion of H_2 in H_2O (Figure 10a), O_2 in H_2O (Figure 10b), and pure H_2O (Figure 10c), respectively.

4. CONCLUSIONS

Extensive MD simulations have been performed to compute the intradiffusion coefficients of (i) H_2 and O_2 in H_2O and (ii) the self-diffusion coefficients of pure H_2O in a wide temperature (275.15−975.15 K) and pressure (0.1−200 MPa) range. Initially, the accuracy of six H_2 and six O_2 force fields was tested to select one force field for each gas for further examination. The TIP4P/2005 force field was used for

https://doi.org/10.1021/acs.jced.1c00300
J. Chem. Eng. Data 2021, 66, 3226−3244

modeling H_2O. The initial screening was based on the accuracy of the force fields in reproducing the available experimentally measured densities, self-diffusivities, and shear viscosities of the pure gas, and the intradiffusivity of the gas in H_2O. During the screening process, experimental measurements that exhibit problematic behavior were identified and appropriate recommendations were introduced. For H_2 and O_2, the force fields by Buch[38] and Bohn et al.[53] were selected, respectively. Subsequently, the selected force fields were used for the computation of the intradiffusion coefficients in the wide temperature and pressure range of interest. Finally, the MD simulation results were used to develop an engineering model with 11 parameters that can estimate the intradiffusion coefficients in vapor, liquid, and supercritical H_2O, with an accuracy of 4−11%. It is expected that the current methodology can be extended to the study of the intradiffusivity of other infinite gases in H_2O. In fact, the following road-map, consisting of four steps, can be utilized for the extension to other gas−H_2O systems: (i) Select appropriate force field for the diffusing gas (solute) based on comparison with the available experimental data for densities, self-diffusivities, and shear viscosities of the pure gas and the intradiffusivity of the gas in H_2O, (ii) perform MD simulations at 3−4 temperatures, for each chosen pressure for the cases of diffusion in H_2O, in the vapor (4 pressures) and liquid (6 pressures) phase, (iii) perform MD simulations at 4−5 temperatures, for each chosen pressure for the cases of diffusion in H_2O, in the supercritical (3 pressures) phase, and (iv) correlate the MD data using eq 8 for the case of diffusion in the vapor or liquid H_2O, and eq 9 for the case in supercritical H_2O.

■ ASSOCIATED CONTENT

Supporting Information

The Supporting Information is available free of charge at https://pubs.acs.org/doi/10.1021/acs.jced.1c00300.

Effect of the number of dissolved hydrogen and oxygen molecules in water in the computed intradiffusivity (Figure S1); finite-size dependency of the computed intradiffusion coefficients of H_2 in liquid, supercritical, and vapor H_2O (Figure S2); Arrhenius-type plots of the computed intradiffusivity of H_2 in H_2O and O_2 in H_2O (Figure S3); plots of densities and shear viscosities of pure water computed with the TIP4P/2005 force field as a function of temperature (Figure S4); force field parameters for water (Table S1), hydrogen (Table S2), and oxygen (Table S3); computed densities of pure hydrogen for different force fields, temperatures, and pressures (Table S4); computed densities of pure oxygen for different force fields, temperatures, and pressures (Table S5); and computed densities (Table S6) and shear viscosities (Table S7) of pure water for different force fields, temperatures, and pressures (PDF)

■ AUTHOR INFORMATION

Corresponding Authors

Ioannis N. Tsimpanogiannis − *Chemical Process & Energy Resources Institute (CPERI), Centre for Research & Technology Hellas (CERTH), 57001 Thermi-Thessaloniki, Greece;* orcid.org/0000-0002-3466-1873; Email: i.n.tsimpanogiannis@certh.gr

Othonas A. Moultos − *Engineering Thermodynamics, Process & Energy Department, Faculty of Mechanical, Maritime and Materials Engineering, Delft University of Technology, 2628CB Delft, The Netherlands;* orcid.org/0000-0001-7477-9684; Email: o.moultos@tudelft.nl

Authors

Samadarshi Maity − *Engineering Thermodynamics, Process & Energy Department, Faculty of Mechanical, Maritime and Materials Engineering, Delft University of Technology, 2628CB Delft, The Netherlands*

Alper T. Celebi − *Engineering Thermodynamics, Process & Energy Department, Faculty of Mechanical, Maritime and Materials Engineering, Delft University of Technology, 2628CB Delft, The Netherlands;* orcid.org/0000-0001-7727-194X

Complete contact information is available at: https://pubs.acs.org/10.1021/acs.jced.1c00300

Notes

The authors declare no competing financial interest.

■ ACKNOWLEDGMENTS

This work was sponsored by NWO Exacte Wetenschappen (Physical Sciences) for the use of supercomputer facilities, with financial support from the Nederlandse Organisatie voor Wetenschappelijk Onderzoek (Netherlands Organisation for Scientific Research, NWO). O.A.M. gratefully acknowledges the support of NVIDIA Corporation with the donation of the Titan V GPU used for this research. This research has been co-financed by the European Regional Development Fund of the European Union and Greek national funds through the Operational Program Competitiveness, Entrepreneurship and Innovation, under the call RESEARCH−CREATE−INNOVATE (project code: T2EDK−01418 Valorization of sugar-beet cultivation residues and by-products of the sugar manufacturing process for the production of bio-based and biocomposite biodegradable packaging materials—Beet2Bioref). I.N.T. gratefully acknowledges partial support from Beet2Bioref.

■ REFERENCES

(1) Jähne, B.; Heinz, G.; Dietrich, W. Measurement of the diffusion coefficients of sparingly soluble gases in water. *J. Geophys. Res.: Oceans* **1987**, *92*, 10767−10776.

(2) Ball, M.; Wietschel, M. The future of hydrogen - opportunities and challenges. *Int. J. Hydrogen Energy* **2009**, *34*, 615−627.

(3) Ursua, A.; Gandia, L. M.; Sanchis, P. Hydrogen Production From Water Electrolysis: Current Status and Future Trends. *Proc. IEEE* **2012**, *100*, 410−426.

(4) Rodriguez Correa, C.; Kruse, A. Supercritical water gasification of biomass for hydrogen production − Review. *J. Supercrit. Fluids* **2018**, *133*, 573−590.

(5) Molino, A.; Larocca, V.; Valerio, V.; Martino, M.; Marino, T.; Rimauro, J.; Casella, P. Biofuels and Bio-based Production via Supercritical Water Gasification of Peach Scraps. *Energy Fuels* **2016**, *30*, 10443−10447.

(6) Guo, L.; Jin, H. Boiling coal in water: Hydrogen production and power generation system with zero net CO_2 emission based on coal and supercritical water gasification. *Int. J. Hydrogen Energy* **2013**, *38*, 12953−12967.

(7) Bermejo, M. D.; Cocero, M. J. Supercritical water oxidation: A technical review. *AIChE J.* **2006**, *52*, 3933−3951.

(8) Marrone, P. A. Supercritical water oxidation—Current status of full-scale commercial activity for waste destruction. *J. Supercrit. Fluids* **2013**, *79*, 283−288.

(9) Himmelblau, D. M. Diffusion of Dissolved Gases in Liquids. *Chem. Rev.* **1964**, *64*, 527−550.
(10) Taylor, R.; Krishna, R. *Multicomponent Mass Transfer*, 1st ed.; John Wiley & Sons: New York, 1993.
(11) Cussler, E. L. *Diffusion: Mass Transfer in Fluid Systems*, 3rd ed.; Cambridge University Press: Cambridge, 2009.
(12) Wilke, C. R.; Chang, P. Correlation of Diffusion Coefficients in Dilute Solutions. *AIChE J.* **1955**, *1*, 264−270.
(13) Boushehri, A.; Bzowski, J.; Kestin, J.; Mason, E. A. Equilibrium and Transport Properties of Eleven Polyatomic Gases At Low Density. *J. Phys. Chem. Ref. Data* **1987**, *16*, 445−466.
(14) Wolff, L.; Jamali, S. H.; Becker, T. M.; Moultos, O. A.; Vlugt, T. J. H.; Bardow, A. Prediction of Composition-Dependent Self-Diffusion Coefficients in Binary Liquid Mixtures: The Missing Link for Darken-Based Models. *Ind. Eng. Chem. Res.* **2018**, *57*, 14784−14794.
(15) Poling, B. E.; Prausnitz, J. M.; O'Connel, J. P. *The Properties of Gases and Liquids*, 5th ed.; McGraw-Hill: Singapore, 2001.
(16) Bird, R. B.; Stewart, W. E.; Lightfoot, E. N. *Transport Phenomena*, 2nd ed.; John Wiley & Sons: New York, 2007.
(17) Brokaw, R. S. Predicting Transport Properties of Dilute Gases. *Ind. Eng. Chem. Process Des. Dev.* **1969**, *8*, 240−253.
(18) García-Pérez, E.; Torréns, I.; Lago, S.; Dubbeldam, D.; Vlugt, T.; Maesen, T.; Smit, B.; Krishna, R.; Calero, S. Elucidating alkane adsorption in sodium-exchanged zeolites from molecular simulations to empirical equations. *Appl. Surf. Sci.* **2005**, *252*, 716−722.
(19) Liu, X.; Bardow, A.; Vlugt, T. J. H. Multicomponent Maxwell-Stefan Diffusivities at Infinite Dilution. *Ind. Eng. Chem. Res.* **2011**, *50*, 4776−4782.
(20) Liu, X.; Schnell, S. K.; Simon, J.-M.; Krüger, P.; Bedeaux, D.; Kjelstrup, S.; Bardow, A.; Vlugt, T. J. H. Diffusion Coefficients from Molecular Dynamics Simulations in Binary and Ternary Mixtures. *Int. J. Thermophys.* **2013**, *34*, 1169−1196.
(21) Allen, M. P.; Tildesley, D. J. *Computer Simulation of Liquids*, 2nd ed.; Oxford University Press: Croydon, 2017.
(22) Frenkel, D.; Smit, B. *Understanding Molecular Simulation: from Algorithms to Applications*, 2nd ed.; Elsevier: San Diego, CA, 2001.
(23) Meunier, M. *Industrial Applications of Molecular Simulations*, 1st ed.; CRC Press: Boca Raton, FL, 2012.
(24) Kallikragas, D. T.; Plugatyr, A. Y.; Svishchev, I. M. High Temperature Diffusion Coefficients for O_2, H_2, and OH in Water, and for Pure Water. *J. Chem. Eng. Data* **2014**, *59*, 1964−1969.
(25) Zhao, X.; Jin, H. Investigation of hydrogen diffusion in supercritical water: A molecular dynamics simulation study. *Int. J. Heat Mass Transfer* **2019**, *133*, 718−728.
(26) Zhao, X.; Jin, H. Correlation for self-diffusion coefficients of H_2, CH_4, CO, O_2 and CO_2 in supercritical water from molecular dynamics simulation. *Appl. Therm. Eng.* **2020**, *171*, No. 114941.
(27) Zhao, X.; Jin, H.; Chen, Y.; Ge, Z. Numerical study of H_2, CH_4, CO, O_2 and CO_2 diffusion in water near the critical point with molecular dynamics simulation. *Comput. Math. Appl.* **2021**, *81*, 759−771.
(28) Xiao, J.; Lu, J.; Chen, J.; Li, Y. Molecular Dynamics Simulation of Diffusion Coefficients of Oxygen, Nitrogen and Sodium Chloride in Supercritical Water. *Chin. Phys. Lett.* **2001**, *18*, 847−849.
(29) Ohmori, T.; Kimura, Y. Anomaly of the temperature dependence of the diffusion of oxygen in supercritical water. *J. Chem. Phys.* **2002**, *116*, 2680−2683.
(30) Ohmori, T.; Kimura, Y. Translational diffusion of hydrophobic solutes in supercritical water studied by molecular dynamics simulations. *J. Chem. Phys.* **2003**, *119*, 7328−7334.
(31) Ge, S.; Zhang, X.; Chen, M. A Molecular Dynamics Simulation of the Diffusivity of O_2 in Supercritical Water. *Int. J. Thermophys.* **2010**, *31*, 2176−2186.
(32) Raman, A. S.; Li, H.; Chiew, Y. C. Widom line, dynamical crossover, and percolation transition of supercritical oxygen via molecular dynamics simulations. *J. Chem. Phys.* **2018**, *148*, No. 014502.
(33) Zhao, X.; Liu, Y.; Zou, J.; Wang, Q.; Liu, H.; Zhang, H.; Jin, H. Determining diffusion coefficients of oxygen in supercritical water with molecular dynamics. *Therm. Sci.* **2019**, *23*, 781−787.
(34) Thapa, S. K.; Adhikari, N. P. A Molecular Dynamics Study of Oxygen Gas in Water at Different Temperatures. *Int. J. Mod. Phys. B* **2013**, *27*, No. 1350023.
(35) Abascal, J. L. F.; Vega, C. A general purpose model for the condensed phases of water: TIP4P/2005. *J. Chem. Phys.* **2005**, *123*, No. 234505.
(36) Tsimpanogiannis, I. N.; Moultos, O. A.; Franco, L. F.; Spera, M. B. d. M.; Erdős, M.; Economou, I. G. Self-diffusion Coefficient of Bulk and Confined Water: A Critical Review of Classical Molecular Simulation Studies. *Mol. Simul.* **2019**, *45*, 425−453.
(37) Tsimpanogiannis, I. N.; Jamali, S. H.; Economou, I. G.; Vlugt, T. J. H.; Moultos, O. A. On the validity of the Stokes−Einstein relation for various water force fields. *Mol. Phys.* **2020**, *118*, No. e1702729.
(38) Buch, V. Path integral simulations of mixed para-D_2 and ortho-D_2 clusters: The orientational effects. *J. Chem. Phys.* **1994**, *100*, 7610−7629.
(39) Köster, A.; Thol, M.; Vrabec, J. Molecular Models for the Hydrogen Age: Hydrogen, Nitrogen, Oxygen, Argon, and Water. *J. Chem. Eng. Data* **2018**, *63*, 305−320.
(40) Hirschfelder, J.; Curtiss, C.; Bird, R. *Molecular Theory of Gases and Liquids*; Wiley, 1954.
(41) Cracknell, R. F. Molecular simulation of hydrogen adsorption in graphitic nanofibres. *Phys. Chem. Chem. Phys.* **2001**, *3*, 2091−2097.
(42) Alavi, S.; Ripmeester, J. A.; Klug, D. D. Molecular-dynamics study of structure II hydrogen clathrates. *J. Chem. Phys.* **2005**, *123*, No. 024507.
(43) Marx, D.; Nielaba, P. Path-integral Monte Carlo techniques for rotational motion in two dimensions: Quenched, annealed, and no-spin quantum-statistical averages. *Phys. Rev. A* **1992**, *45*, 8968−8971.
(44) Rahbari, A.; Brenkman, J.; Hens, R.; Ramdin, M.; van den Broeke, L. J. P.; Schoon, R.; Henkes, R.; Moultos, O. A.; Vlugt, T. J. H. Solubility of Water in Hydrogen at High Pressures: A Molecular Simulation Study. *J. Chem. Eng. Data* **2019**, *64*, 4103−4115.
(45) Rahbari, A.; Garcia-Navarro, J. C.; Ramdin, M.; van den Broeke, L. J. P.; Moultos, O. A.; Dubbeldam, D.; Vlugt, T. J. H. Effect of water content on thermodynamic properties of compressed hydrogen. *J. Chem. Eng. Data* **2021**, *66*, 2071−2087.
(46) Luis, D. P.; Romero-Ramirez, I. E.; González-Calderón, A.; López-Lemus, J. The coexistence temperature of hydrogen clathrates: A molecular dynamics study. *J. Chem. Phys.* **2018**, *148*, No. 114503.
(47) Papadimitriou, N. I.; Tsimpanogiannis, I. N.; Papaioannou, A. T.; Stubos, A. K. Evaluation of the Hydrogen-Storage Capacity of Pure H_2 and Binary H_2-THF Hydrates with Monte Carlo Simulations. *J. Phys. Chem. C* **2008**, *112*, 10294−10302.
(48) Papadimitriou, N. I.; Tsimpanogiannis, I. N.; Economou, I. G.; Stubos, A. K. Storage of H_2 in Clathrate Hydrates: Evaluation of Different Force-Fields used in Monte Carlo Simulations. *Mol. Phys.* **2017**, *115*, 1274−1285.
(49) Tsimpanogiannis, I. N.; Economou, I. G. Monte Carlo simulation studies of clathrate hydrates: A review. *J. Supercrit. Fluids* **2018**, *134*, 51−60.
(50) Yang, X.; Xu, J.; Wu, S.; Yu, M.; Hu, B.; Cao, B.; Li, J. A molecular dynamics simulation study of PVT properties for $H_2O/H_2/CO_2$ mixtures in near-critical and supercritical regions of water. *Int. J. Hydrogen Energy* **2018**, *43*, 10980−10990.
(51) Bartolomeu, R. A.; Franco, L. F. Thermophysical properties of supercritical H_2 from Molecular Dynamics simulations. *Int. J. Hydrogen Energy* **2020**, *45*, 16372−16380.
(52) Bartolomeu, R. A. C.; Lopes, J. T.; Spera, M. B. M.; Franco, L. F. M. Derivative Properties Data for Hydrogen−Ethylene Supercritical Mixtures Using a SAFT EoS and a SAFT Force Field. *J. Chem. Eng. Data* **2020**, *65*, 5735−5742.
(53) Bohn, M.; Lustig, R.; Fischer, J. Description of polyatomic real substances by two-center Lennard-Jones model fluids. *Fluid Phase Equilib.* **1986**, *25*, 251−262.

https://doi.org/10.1021/acs.jced.1c00300
J. Chem. Eng. Data 2021, 66, 3226−3244

(54) Miyano, Y. Molecular simulation with an EOS algorithm for vapor-liquid equilibria of oxygen and ethane. *Fluid Phase Equilib.* **1999**, *158−160*, 29−35.
(55) Coon, J. E.; Gupta, S.; McLaughlin, E. Isothermalisobaric molecular dynamics simulation of diatomic liquids and their mixtures. *Chem. Phys.* **1987**, *113*, 43−52.
(56) Hansen, N.; Agbor, F. A.; Keil, F. J. New force fields for nitrous oxide and oxygen and their application to phase equilibria simulations. *Fluid Phase Equilib.* **2007**, *259*, 180−188.
(57) Vrabec, J.; Stoll, J.; Hasse, H. A set of molecular models for symmetric quadrupolar fluids. *J. Phys. Chem. B* **2001**, *105*, 12126−12133.
(58) Watanabe, K.; Austin, N.; Stapleton, M. R. Investigation of the air separation properties of zeolites types a, x and y by monte carlo simulations. *Mol. Simul.* **1995**, *15*, 197−221.
(59) Vega, C.; Abascal, J. L. F. Simulating Water with Rigid Non-polarizable Models: A General Perspective. *Phys. Chem. Chem. Phys.* **2011**, *13*, 19663−19688.
(60) Michalis, V. K.; Moultos, O. A.; Tsimpanogiannis, I. N.; Economou, I. G. Molecular Dynamics Simulations of the Diffusion Coefficients of Light n-alkanes in Water over a Wide Range of Temperature and Pressure. *Fluid Phase Equilib.* **2016**, *407*, 236−242.
(61) Döpke, M. F.; Moultos, O. A.; Hartkamp, R. On the transferability of ion parameters to the TIP4P/2005 water model using molecular dynamics simulations. *J. Chem. Phys.* **2020**, *152*, No. 024501.
(62) González, M. A.; Abascal, J. L. The Shear Viscosity of Rigid Water Models. *J. Chem. Phys.* **2010**, *132*, No. 096101.
(63) Jiang, H.; Moultos, O. A.; Economou, I. G.; Panagiotopoulos, A. Z. Hydrogen-bonding Polarizable Intermolecular Potential Model for Water. *J. Phys. Chem. B* **2016**, *120*, 12358−12370.
(64) Moultos, O.; Tsimpanogiannis, I.; Panagiotopoulos, A.; Economou, I. Atomistic molecular dynamics simulations of CO_2 diffusivity in H_2O for a wide range of temperatures and pressures. *J. Phys. Chem. B* **2014**, *118*, 5532−5541.
(65) Zeron, I. M.; Gonzalez, M. A.; Errani, E.; Vega, C.; Abascal, J. L. F. "In Silico" Seawater. *J. Chem. Theory Comput.* **2021**, *17*, 1715−1725.
(66) Moultos, O. A.; Tsimpanogiannis, I. N.; Panagiotopoulos, A. Z.; Economou, I. G. Self-Diffusion Coefficients of the Binary (H_2O + CO_2) Mixture at High Temperatures and Pressures. *J. Chem. Thermodyn.* **2016**, *93*, 424−429.
(67) Plimpton, S. Short-Range Molecular Dynamics. *J. Comput. Phys.* **1997**, *117*, 1−42.
(68) Ryckaert, J. P.; Ciccotti, G.; Berendsen, H. J. Numerical integration of the cartesian equations of motion of a system with constraints: molecular dynamics of n-alkanes. *J. Comput. Phys.* **1977**, *23*, 327−341.
(69) Zhang, Z.; Glotzer, S. C. Self-assembly of patchy particles. *Nano Lett.* **2004**, *4*, 1407−1413.
(70) Hockney, R. W.; Eastwood, J. W. *Computer Simulation Using Particles*; Adam Hilger: New York, 1989.
(71) Jamali, S. H.; Wolff, L.; Becker, T. M.; de Groen, M.; Ramdin, M.; Hartkamp, R.; Bardow, A.; Vlugt, T. J. H.; Moultos, O. A. OCTP: A Tool for On-the-fly Calculation of Transport Properties of Fluids with the Order-n Algorithm in LAMMPS. *J. Chem. Inf. Model.* **2019**, *59*, 1290−1294.
(72) Kamberaj, H.; Low, R. J.; Neal, M. P. Time reversible and symplectic integrators for molecular dynamics simulations of rigid molecules. *J. Chem. Phys.* **2005**, *122*, No. 224114.
(73) Martínez, L.; Andrade, R.; Birgin, E. G.; Martínez, J. M. PACKMOL: A Package for Building Initial Configurations for Molecular Dynamics Simulations. *J. Comput. Chem.* **2009**, *30*, 2157−2164.
(74) Mondello, M.; Grest, G. S. Viscosity Calculations of n-Alkanes by Equilibrium Molecular Dynamics. *J. Chem. Phys.* **1997**, *106*, 9327−9336.
(75) Krishna, R.; van Baten, J. M. The Darken Relation for Multicomponent Diffusion in Liquid Mixtures of Linear Alkanes: An Investigation Using Molecular Dynamics (MD) Simulations. *Ind. Eng. Chem. Res.* **2005**, *44*, 6939−6947.
(76) Tenney, C. M.; Maginn, E. J. Limitations and Recommendations for the Calculation of Shear Viscosity using Reverse Non-equilibrium Molecular Dynamics. *J. Chem. Phys.* **2010**, *132*, No. 014103.
(77) Dubbeldam, D.; Ford, D. C.; Ellis, D. E.; Snurr, R. Q. A New Perspective on the Order-n Algorithm for Computing Correlation Functions. *Mol. Simul.* **2009**, *35*, 1084−1097.
(78) Meador, W. E.; Miner, G. A.; Townsend, L. W. Bulk viscosity as a relaxation parameter: Fact or fiction? *Phys. Fluids* **1996**, *8*, 258−261.
(79) Hagen, M. H. J.; Lowe, C. P.; Frenkel, D. In *Long Time Tails in Stress Correlation Functions*, 25 Years of Non-Equilibrium Statistical Mechanics, Berlin, Heidelberg, 2005; pp 240−249.
(80) Janzen, T.; Zhang, S.; Mialdun, A.; Guevara-Carrion, G.; Vrabec, J.; He, M.; Shevtsova, V. Mutual Diffusion Governed by Kinetics and Thermodynamics in the Partially Miscible Mixture Methanol + Cyclohexane. *Phys. Chem. Chem. Phys.* **2017**, *19*, 31856−31873.
(81) Guevara-Carrion, G.; Ancherbak, S.; Mialdun, A.; Vrabec, J.; Shevtsova, V. Diffusion of Methane in Supercritical Carbon Dioxide Across the Widom Line. *Sci. Rep.* **2019**, *9*, No. 8466.
(82) Yeh, I.-C.; Hummer, G. System-size Dependence of Diffusion Coefficients and Viscosities from Molecular Dynamics Simulations with Periodic Boundary Conditions. *J. Phys. Chem. B* **2004**, *108*, 15873−15879.
(83) Celebi, A. T.; Jamali, S. H.; Bardow, A.; Vlugt, T. J. H.; Moultos, O. A. Finite-size Effects of Diffusion Coefficients Computed from Molecular Dynamics: A Review of What we have Learned so far *Mol. Simul.* 2021, DOI: 10.1080/08927022.2020.1810685, in press.
(84) Jamali, S. H.; Bardow, A.; Vlugt, T. J. H.; Moultos, O. A. Generalized Form for Finite-Size Corrections in Mutual Diffusion Coefficients of Multicomponent Mixtures Obtained from Equilibrium Molecular Dynamics Simulation. *J. Chem. Theory Comput.* **2020**, *16*, 3799−3806.
(85) Jamali, S. H.; Hartkamp, R.; Bardas, C.; Söhl, J.; Vlugt, T. J. H.; Moultos, O. A. Shear viscosity computed from the finite-size effects of self-diffusivity in equilibrium molecular dynamics. *J. Chem. Theory Comput.* **2018**, *14*, 5959−5968.
(86) Moultos, O. A.; Zhang, Y.; Tsimpanogiannis, I. N.; Economou, I. G.; Maginn, E. J. System-size Corrections for Self-diffusion Coefficients Calculated from Molecular Dynamics Simulations: The Case of CO_2, n-alkanes, and Poly (Ethylene Glycol) Dimethyl Ethers. *J. Chem. Phys.* **2016**, *145*, No. 074109.
(87) Jamali, S. H.; Wolff, L.; Becker, T. M.; Bardow, A.; Vlugt, T. J. H.; Moultos, O. A. Finite-size Effects of Binary Mutual Diffusion Coefficients from Molecular Dynamics. *J. Chem. Theory Comput.* **2018**, *14*, 2667−2677.
(88) Dünweg, B.; Kremer, K. Molecular dynamics simulation of a polymer chain in solution. *J. Chem. Phys.* **1993**, *99*, 6983−6997.
(89) Erdős, M.; Frangou, M.; Vlugt, T. J.; Moultos, O. A. Diffusivity of α-, β-, γ-cyclodextrin and the inclusion complex of β-cyclodextrin: Ibuprofen in aqueous solutions; A molecular dynamics simulation study. *Fluid Phase Equilib.* **2021**, *528*, No. 112842.
(90) Lemmon, E. W.; Bell, I. H.; Huber, M. L.; McLinden, M. O. NIST Standard Reference Database 23: Reference Fluid Thermodynamic and Transport Properties-REFPROP, Version 10.0, National Institute of Standards and Technology, 2018.
(91) Chen, L.; Groß, T.; Krienke, H.; Lüdemann, H.-D. T,p-Dependence of the self-diffusion and spin−lattice relaxation in fluid hydrogen and deuterium. *Phys. Chem. Chem. Phys.* **2001**, *3*, 2025−2030.
(92) Winn, E. B. The Temperature Dependence of the Self-Diffusion Coefficients of Argon, Neon, Nitrogen, Oxygen, Carbon Dioxide, and Methane. *Phys. Rev.* **1950**, *80*, 1024−1027.
(93) Winkelmann, J. *Landolt-Börnstein: Numerical Data and Functional Relationships in Science and Technology, Group IV: Physical Chemistry Volume 15, Subvolume A: Gases in Gases, Liquids and their Mixtures*; Springer-Verlag: Berlin, Heidelberg, New York, 2007.

(94) Gertz, K. H.; Loeschcke, H. H. Bestimmung der Diffusions-Koeffizienten von H_2, O_2, N_2, und He in Wasser und Blutserum bei konstant gehaltener Konvektion. *Z. Naturforsch. B* **1954**, *9*, 1−9.
(95) Baird, M. H.; Davidson, J. F. Annular jets—II: Gas absorption. *Chem. Eng. Sci.* **1962**, *17*, 473−480.
(96) Wise, D. L.; Houghton, G. The diffusion coefficients of ten slightly soluble gases in water at 10−60 °C. *Chem. Eng. Sci.* **1966**, *21*, 999−1010.
(97) Akgerman, A.; Gainer, J. L. Predicting gas-liquid diffusivities. *J. Chem. Eng. Data* **1972**, *17*, 372−377.
(98) de Blok, W. J.; Fortuin, J. M. H. Method for determining diffusion coefficients of slightly soluble gases in liquids. *Chem. Eng. Sci.* **1981**, *36*, 1687−1694.
(99) Verhallen, P.; Oomen, L.; Elsen, A.; Kruger, J.; Fortuin, J. The diffusion coefficients of helium, hydrogen, oxygen and nitrogen in water determined from the permeability of a stagnant liquid layer in the quasi-steady state. *Chem. Eng. Sci.* **1984**, *39*, 1535−1541.
(100) Ferrell, R. T.; Himmelblau, D. M. Diffusion coefficients of nitrogen and oxygen in water. *J. Chem. Eng. Data* **1967**, *12*, 111−115.
(101) Han, P.; Bartels, D. M. Temperature Dependence of Oxygen Diffusion in H_2O and D_2O. *J. Phys. Chem. R* **1996**, *100*, 5597−5602.
(102) Roetzel, W.; Blomker, D.; Czarnetzki, W. Messung binarer Diffusionskoeffizienten von Gasen in Wasser mit Hilfe der holographischen Interferometrie. *Chem. Ing. Tech.* **1997**, *69*, 674−678.
(103) Wagner, W.; Pruss, A. International Equations for the Saturation Properties of Ordinary Water Substance. Revised According to the International Temperature Scale of 1990. Addendum to J. Phys. Chem. Ref. Data 16, 893 (1987). *J. Phys. Chem. Ref. Data* **1993**, *22*, 783−787.
(104) Wiebe, R.; Gaddy, V. L.; Heins, C. Solubility of Hydrogen in Water at 250c from 25 to 1000 Atmospheres. *Ind. Eng. Chem.* **1932**, *24*, 823−825.
(105) Wiebe, R.; Gaddy, V. L. The Solubility of Hydrogen in Water at 0, 50, 75 and 100° from 25 to 1000 Atmospheres. *J. Am. Chem. Soc.* **1934**, *56*, 76−79.
(106) Battino, R. *IUPAC Solubility Data Series. vol 7. Hydrogen and Deuterium*, 1st ed.; Pergamon Press: Oxford, 1981.
(107) Young, C. L. *IUPAC Solubility Data Series. vol 5/6. Oxygen and Ozone*, 1st ed.; Pergamon Press: Oxford, 1981.
(108) Dawass, N.; Krüger, P.; Schnell, S. K.; Simon, J.-M.; Vlugt, T. Kirkwood-Buff Integrals from Molecular Simulation. *Fluid Phase Equilib.* **2019**, *486*, 21−36.
(109) Dawass, N.; Krüger, P.; Schnell, S. K.; Moultos, O. A.; Economou, I. G.; Vlugt, T. J. H.; Simon, J.-M. Kirkwood-Buff Integrals Using Molecular Simulation: Estimation of Surface Effects. *Nanomaterials* **2020**, *10*, No. 771.
(110) Krynicki, K.; Green, C. D.; Sawyer, D. W. Pressure and temperature dependence of self-diffusion in water. *Faraday Discuss. Chem. Soc.* **1978**, *66*, 199−208.
(111) Guevara-Carrion, G.; Vrabec, J.; Hasse, H. Prediction of self-diffusion coefficient and shear viscosity of water and its binary mixtures with methanol and ethanol by molecular simulation. *J. Chem. Phys.* **2011**, *134*, No. 074508.
(112) Berendsen, H. J. C.; Grigera, J. R.; Straatsma, T. P. The missing term in effective pair potentials. *J. Phys. Chem. R* **1987**, *91*, 6269−6271.
(113) Kawasaki, K.; Oppenheim, I. Logarithmic Term in the Density Expansion of Transport Coefficients. *Phys. Rev.* **1965**, *139*, A1763−A1768.
(114) Yang, Q.; Zhong, C. Molecular Simulation of Adsorption and Diffusion of Hydrogen in Metal-Organic Frameworks. *J. Phys. Chem. B* **2005**, *109*, 11862−11864.
(115) Brooks, B. R.; et al. CHARMM: The biomolecular simulation program. *J. Comput. Chem.* **2009**, *30*, 1545−1614.

https://doi.org/10.1021/acs.jced.1c00300
J. Chem. Eng. Data 2021, 66, 3226−3244